Magnetic Fields

Neutron stars are expected to have strong B-fields!

Neutron stars are formed in supernova explosions.

One of the conserved quantities is the magnetic flux,

$$\Phi = 4\pi R^2 B \quad \Longrightarrow \quad R_{\mathrm{NS}}^2 B_{\mathrm{NS}} = R_*^2 B_* \tag{5.1}$$

or

$$B_{\mathrm{NS}} = B_* \left(\frac{R_*}{R_{\mathrm{NS}}} \right)^2 \tag{5.2}$$

with $R_* \sim 700000\,\mathrm{km}$, $R_{\mathrm{NS}} = 10\,\mathrm{km}$ and typical pre supernova stellar B-fields of $B_* \sim 100\,\mathrm{G}$, giving $B_{\mathrm{NS}} = 5 \times 10^9 \times 10^2\,\mathrm{G} = 5 \times 10^{11}\,\mathrm{G}$.

Young Neutron Stars are expected to have magnetic fields on the order of $10^{12}\,\mathrm{G}$ ($10^8\,\mathrm{T}$).

Theories in which neutron star magnetic fi elds are formed after the supernova yield similar results.

$\Longrightarrow$ Will look at young neutron stars, i.e. High Mass X-ray Binaries.

High Mass X-ray Binaries

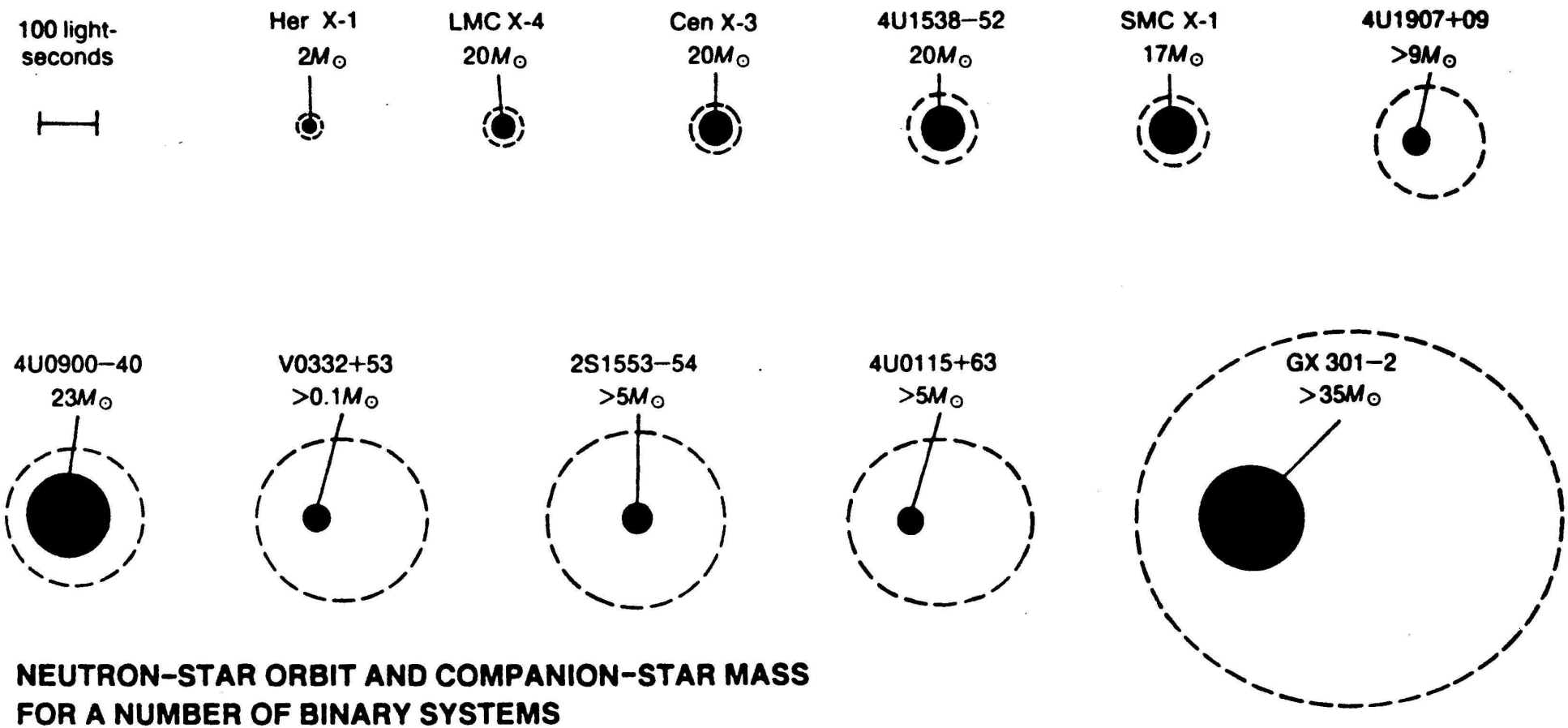

NEUTRON-STAR ORBIT AND COMPANION-STAR MASS FOR A NUMBER OF BINARY SYSTEMS

Charles & Seward (1995, Fig. 7.7a)

High-Mass X-ray Binaries: Donor star has early spectral type (O, B), and mass $M \gtrsim 6\,M_\odot$, wind accreters, Roche lobe overflow, or Be accretion.

Be Accretion

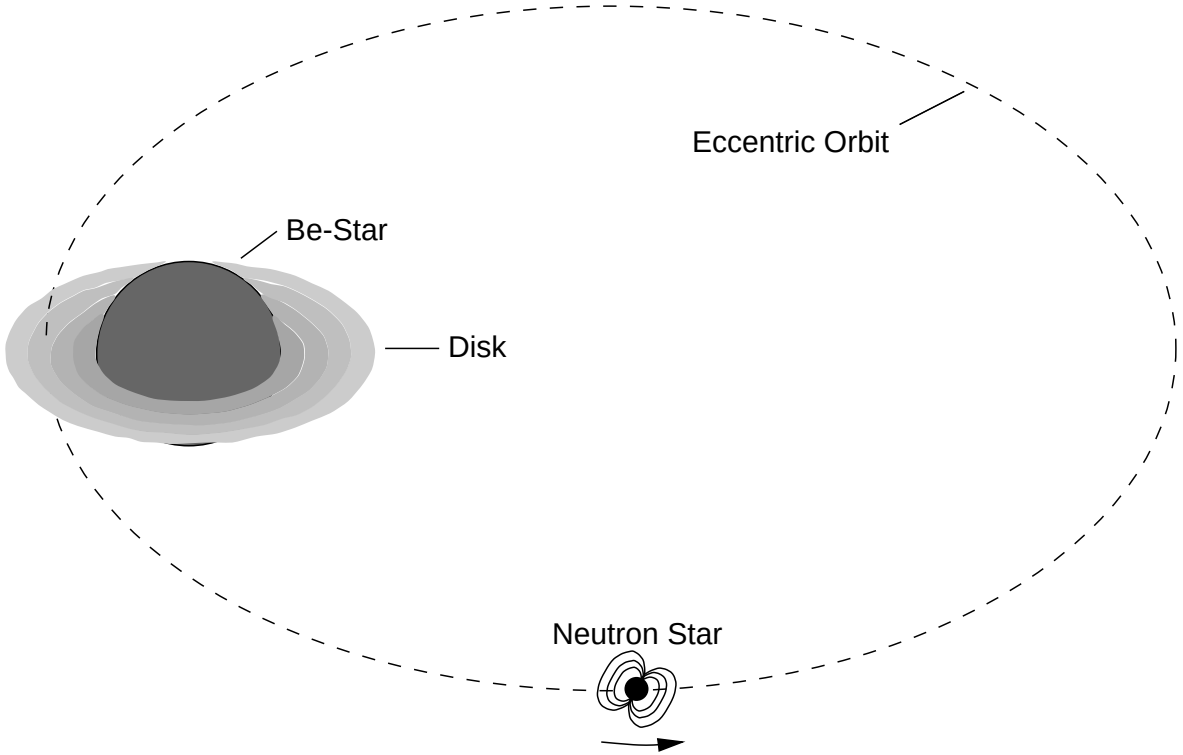

(Kretschmar 1996, Dissertation AIT, Abb. 2.6)

Some early type stars (O9–B2) have very high rotation rates $\Longrightarrow$ Formation of disk-like stellar wind at equator. Line emission from disk: Be phenomenon.

Collision of neutron star with disk results in irregular X-ray outbursts.

Example: A0535+26.

Table 1.3. *The orbital periods of HMXBs*

Source	Alternative name	Orbital period (d)	Properties[a]	Reference
X2030+407	Cyg X–3	0.2	WR	1,2,3
X0532–664	LMC X–4	1.4	SG, P	4,5,6
X0538–641	LMC X–3	1.7	Be, BHC	7
X1119–603	Cen X–3	2.1	SG, P	8
X1700–377	HD153919	3.41	SG	9
X1538–522	QV Nor	3.73	SG, P	10,11
X0115–737	SMC X–1	3.89	SG, P	12
X0540–697	LMC X–1	4.22	SG, BHC	13
X1956+350	Cyg X–1	5.6	SG, BHC	14
X1907+097		8.38	B, P	15
X0900–403	Vela X–1	8.96	SG, P	16
X1657–415		10.4	SG?, P	17
X0114+650	V662 Cas	11.6	SG	18
X1909+048	SS433	13.1	SG, J	19
X0535–668	A0538–66	16.7	Be, T, P	20
X0115+634	V635 Cas	24.3	Be, T, P	21
X0236+610	LS I +61 303	26.45	Be	22
X1553–542		30.6	Be?, T, P	23
X0331+530	BQ Cam	34.25	Be, T, P	24
X1223–624	GX301–2	41.5	SG, P	25,26,27
X2030+375		45–47	Be, T, P	28
X0535+262	HD245770	111	Be, T, P	29
X1258–613	GX304–1	133?	Be, P	30
X1145–619	Hen 715	187.5	Be, P	31

[a]The source properties are indicated by 'SG' - supergiant, 'Be' - Be star, 'P' - pulsar, 'BHC' - black-hole candidate, 'T' - transient, 'WR' - Wolf–Rayet, 'J' - Jets.

References: [1]Parsignault *et al.* 1972; [2]Sanford & Hawkins 1972; [3]van Kerkwijk *et al.* 1992; [4]Li *et al.* 1978; [5]White 1978; [6]Chevalier & Ilovaisky 1977; [7]Cowley *et al.* 1983; [8]Schreier *et al.* 1972b; [9]Jones, Forman and Liller 1973; [10]Becker *et al.* 1977; [11]Davison, Watson and Pye 1977; [12]Schreier *et al.* 1972b; [13]Hutchings *et al.* 1983; [14]Webster & Murdin 1972; [15]Marshall & Ricketts 1980; [16]Ulmer *et al.* 1972; [17]Chakrabarty *et al.* 1993; [18]Crampton *et al.* 1985; [19]Crampton *et al.* 1980; [20]Johnston, *et al.* 1980; [21]Rappaport *et al.* 1978; [22]Taylor & Gregory 1982; [23]Kelley *et al.* 1983b; [24]Stella *et al.* 1985; [25]Watson *et al.* 1982; [26]Kelley *et al.* 1980; [27]White *et al.* 1978; [28]Parmar *et al.* 1989c,d; [29]Priedhorsky & Terrell 1983a; [30]Priedhorsky & Terrell 1983b; [31]Watson *et al.* 1981.

White et al., 1995, Tab. 1.3

Table 1.4. *Pulse periods from X-ray binaries*

Source	Alternative name	Pulse period (s)	Orbital period (d)	Type	Reference
X0535−668	A0538−66	0.069	16.7	HMXB	1
X0115−737	SMC X−1	0.71	3.89	HMXB	2
X1656+354	Her X−1	1.24	1.7	LMXB	3
X0115+634	V635 Cas	3.6	24.3	HMXB	4
X0332+530	BQ Cam	4.4	34.25	HMXB	5
X1119−603	Cen X−3	4.8	2.1	HMXB	6
X1048−594		6.4		?	7
X2259+587		7.0		LMXB	8
X1627−673		7.7	0.029	LMXB	9
X1553−542		9.3	30.6	HMXB	10
X0834−430	GR0834−430	12.2	-	?	11
X0532−664	LMC X−4	13.5	1.4	HMXB	12
X1417−624		17.6		HMXB	13
X1843+009		29.5		?	14
X1657−415		38	10.4	HMXB	15
X2030+375		42	45.6	HMXB	16
X2138+568	Cep X−4	66		?	17
X1836−045		81		?	14
X1843−024		95		?	14,34
X0535+262		104	111	HMXB	18
X1833−076	Sct X−1	111		?	19
X1728−247	GX1+4	114	304?	LMXB	20,21,22
X0900−403	Vela X−1	283	8.96	HMXB	23
X1258−613	GX 304−1	272	133?	HMXB	24,25
X1145−614		298		HMXB	26,27
X1145−619		292	187.5	HMXB	26,27
X1118−615	A1118−61	405		HMXB	28
X1722−363		413		?	29
X1907+097		438	8.38	HMXB	30
X1538−522	QV Nor	529	3.73	HMXB	31
X1223−624	GX301−2	696	41.5	HMXB	32
X0352−309	X Per	835		HMXB	33

References: [1]Skinner *et al.* 1982; [2]Lucke *et al.* 1976; [3]Tananbaum *et al.* 1972; [4]Cominsky *et al.* 1978; [5]Stella *et al.* 1985; [6]Giacconi *et al.* 1971; [7]Corbet & Day 1990; [8]Gregory & Fahlman 1980; [9]Rappaport *et al.* 1977; [10]Kelley *et al.* 1983b; [11]Grebenev & Sunyaev 1991; [12]Kelley *et al.* 1983a; [13]Kelley *et al.* 1981; [14]Koyama *et al.* 1990a; [15]White & Pravdo 1979; [16]Parmar *et al.* 1989d; [17]Koyama *et al.* 1991a; [18]Rosenberg *et al.* 1975; [19]Koyama *et al.* 1991b; [20]Lewin *et al.* 1971; [21]White *et al.* 1976a; [22]Strickman *et al.* 1980; [23]McClintock *et al.* 1976; [24]Huckle *et al.* 1977; [25]McClintock *et al.* 1977; [26]White *et al.* 1978b; [27]Lamb *et al.* 1980; [28]Ives *et al.* 1975; [29]Tawara *et al.* 1989; [30]Makishima *et al.* 1984; [31]Davison *et al.* 1977; [32]White *et al.* 1976a; [33]White *et al.* 1976b; [34]Koyama *et al.* 1990b.

White et al., 1995, Tab. 1.4

Table 1: Known Accretion-Powered Pulsars (as of Feb. 1997)

	System[a]	l_{II}	b_{II}	P_{spin} (s)	P_{orb}[b] (d)	Companion (MK Type)	References[d]
	Low-mass binaries						
⊙	GRO J1744–28	0.0	+0.3	0.467	11.8		[1]
•	Her X-1	58.2	+37.5	1.24	1.70	HZ Her (A9-B)	[2],[3]
•	4U 1626–67	321.8	-13.1	7.66	0.0289	KZ TrA (low-mass dwarf)	[4],[5]
•	4U 1728–247 (GX 1+4)	1.9	+4.8	120		V2116 Oph (M6III)	[6],[7]
	High-mass supergiant and giant systems						
	SMC X-1	300.4	-43.6	0.717	3.89	Sk160 (B0 I)	[8]
•	Cen X-3	292.1	+0.3	4.82	2.09	V779 Cen (O6–8f)	[9],[10]
	RX J0648.1–4419	253.7	-19.1	13.2	1.54	HD 49798 (O6p)	[11]
	LMC X-4	276.3	-32.5	13.5	1.41	Sk-Ph (O7 III-V)	[12]
•	OAO 1657–415	344.4	+0.3	37.7	10.4	(B0–6lab)	[13]
•	Vela X-1	263.1	+3.9	283	8.96	HD77581 (B0.5Ib)	[14]
	1E 1145–614	295.5	-0.0	297	5.65	V830 Cen (B2Iae)	[15]
	4U 1907+09	43.7	+0.5	438	8.38	(B I)	[16]
•	4U 1538–52	327.4	+2.1	530	3.73	QV Nor (B0Iab)	[17],[18]
•	GX 301–2	300.1	-0.0	681	41.5	Wray 977 (B1.5Ia)	[19],[20]
	Transient Be-binary systems						
	A 0538–67	276.9	-32.2	0.069	16.7	(B2 III-IVe)	[21]
•	4U 0115+63	125.9	+1.0	3.61	24.3	V635 Cas (Be)	[22],[23]
	V 0332+53	146.1	-2.2	4.37	34.2	BQ Cam (Be)	[24]
•	2S 1417–624	313.0	-1.6	17.6	42.1	(OBe)	[25]
•	EXO 2030+375	77.2	-1.3	41.7	46.0	(Be)	[26],[27]
⊙	GRO J1008–57	283.0	-1.8	93.5	≈ 248	(Be)	[28],[29]
•	A 0535+26	181.4	-2.6	105	110	HDE245770 (O9.7IIe)	[30]
	GX 304–1	302.1	+1.2	272	133 (?)	V 850 Cen (B2Vne)	[31]
•	4U 1145–619	295.6	-0.2	292	187	Hen715 (B1Vne)	[32]
•	A 1118–616	292.5	-0.9	405		He3-640 (O9.5 III-Ve)	[33]
	4U 0352+309	163.1	-17.1	835		X Per (O9 III-Ve)	[34]
	RX J0146.9+6121	129.9	-0.5	1413		LSI +61° 235 (B5 IIIe)	[35]
	Persistent systems with an undetermined companion						
	RX J1838.4–0301	28.8	+1.5	5.45			[36]
	1E 1048–593	288.2	-0.5	6.44			[37]
	1E 2259+586	109.1	-1.0	6.98			[38]
	RX J0720.4-3125	244.2	-8.2	8.38			[39]
	4U 0142+614	129.4	-0.4	8.69			[40]
	Transient systems with an undetermined companion						
•	RX J0059.2–7138[c]	302.1	-45.5	2.76			[41]
	RX J0502.9–6626	277.0	-35.5	4.06			[42]
⊙	GRO J1750–27	2.4	+0.5	4.45	29.8		[43]
	2E 0050.1–7247	302.9	-44.6	8.9			[11]
	2S 1553–54	327.9	-0.9	9.26	30.6		[44]
•	GS 0834–430	262.0	-1.5	12.3	106		[45],[46]
⊙	GRO J1948+32	64.9	1.8	18.7			[47]
	GS 1843+00	33.1	+1.7	29.5			[48]
	GS 2138+56 (Cep X-4?)	99.0	+3.3	66.2			[49]
	GS 1843–024	30.2	-0.0	94.8			[50]
	Sct X-1	24.5	-0.2	111			[51]
⊙	GRO J2058+42	83.6	-2.7	198	≈110		[52],[53]
	GPS 1722–363	351.5	-0.6	414			[54]

[a] Sources marked • have been detected with BATSE, sources marked with ⊙ were discovered by BATSE.

[b] In those cases where no orbital parameters are given in Table 3, the orbital period has been inferred from pulse timing and/or outburst recurrence times and/or optical photometry.

[c] This source was detected by both BATSE and ROSAT on MJD 49120. It has not been studied with BATSE and is not discussed in this paper.

[d] REFERENCES: [1] Finger et al.1996; [2] Decter et al.1991; [3] Wilson et al.1994a; [4] Chakrabarty et al.1997a; [5] Middleditch et al.1981; [6] Chakrabarty et al.1997b; [7] Makishima et al.1988; [8] Levine et al.1993; [9] Finger et al.1993; [10] Nagase et al.1992; [11] Israel et al.1995; [12] Safi-Harb, Ogelman & Dennerl 1996; [13] Chakrabarty et al.1993; [14] Decter et al.1987; [15] Ilovaisky, Chevalier & Motch 1982; [16] Makishima et al.1984; [17] Rubin et al.1994; [18] Corbet et al.1993; [19] Koh et al.1997; [20] Sato et al.1986; [21] Skinner 1981; [22] Cominsky et al.1994; [23] Rappaport et al.1978; [24] Stella et al.1985; [25] Finger, Wilson & Chakrabarty 1996; [26] Stollberg et al.1994; [27] Parmar et al.1989; [28] Wilson et al.1994b; [29] Coe et al.1994a; [30] Finger, Wilson & Harmon 1996; [31] Priedhorsky & Terrell 1983; [32] Cook & Warwick 1987; [33] Ives, Sanford & Bell-Burnell 1975; [34] Murakami et al.1987; [35] Hellier 1994; [36] Schwentker 1994; [37] Seward, Charles & Smale 1986; [38] Iwasawa, Koyama & Halpern 1992; [39] Haberl et al.1996; [40] Israel, Mereghetti, & Stella 1994; [41] Hughes 1994; [42] Schmidtke et al.1995; [43] Scott et al., in preparation; [44] Kelley, Rappaport and Ayasli 1983; [45] Wilson et al.1997; [46] Aoki et al.1992; [47] Chakrabarty et al.1995; [48] Koyama et al.1990a; [49] Koyama et al.1991a; [50] Koyama et al.1990b; [51] Koyama et al.1991b; [52] Wilson, Strohmayer & Chakrabarty 1996; [53] Wilson et al.1995a; [54] Tawara et al.1989.

Magnetospheric accretion, I

Accretion models has to take into account that central neutron star has $\sim 10^{12}$ G B-field.

Far-field:

$$B(r) = \left(\frac{R}{r}\right)^3 B_\mathrm{p} \quad \text{hence} \quad P_\mathrm{mag} = \frac{B^2}{8\pi} = \left(\frac{R}{r}\right)^6 B_\mathrm{p}^2$$

On the other hand, the accreting material has a ram-pressure

$$P_\mathrm{ram} = \rho v^2 \quad \text{or} \quad P_\mathrm{ram} = \frac{\dot{M}}{4\pi r^2}\left(\frac{2GM}{r}\right)^{1/2}$$

assuming free fall ($v = (2GM/r)^{1/2}$) and spherical symmetry ($\dot{M} = 4\pi r^2 \rho v$).

For $P_\mathrm{mag} > P_\mathrm{ram}$, B-field dominates $\Longrightarrow$ plasma couples to B-field lines at the Alfvén radius

$$r_\mathrm{mag} = \left(\frac{8\pi^2}{G}\right)^{1/7}\left(\frac{R^{12}B_\mathrm{p}^4}{M\dot{M}^2}\right)^{1/7}$$

$$= 1800\,\mathrm{km}\left(\frac{R}{10\,\mathrm{km}}\right)^{12/7}\left(\frac{B}{10^{12}\,\mathrm{G}}\right)^{4/7}\left(\frac{M}{1.4\,M_\odot}\right)^{-1/7}\left(\frac{\dot{M}}{10^{-7}\,M_\odot\,\mathrm{yr}^{-1}}\right)^{-2/7}$$

For typical NS parameters, the accretion close to the NS is dominated by the B-field.

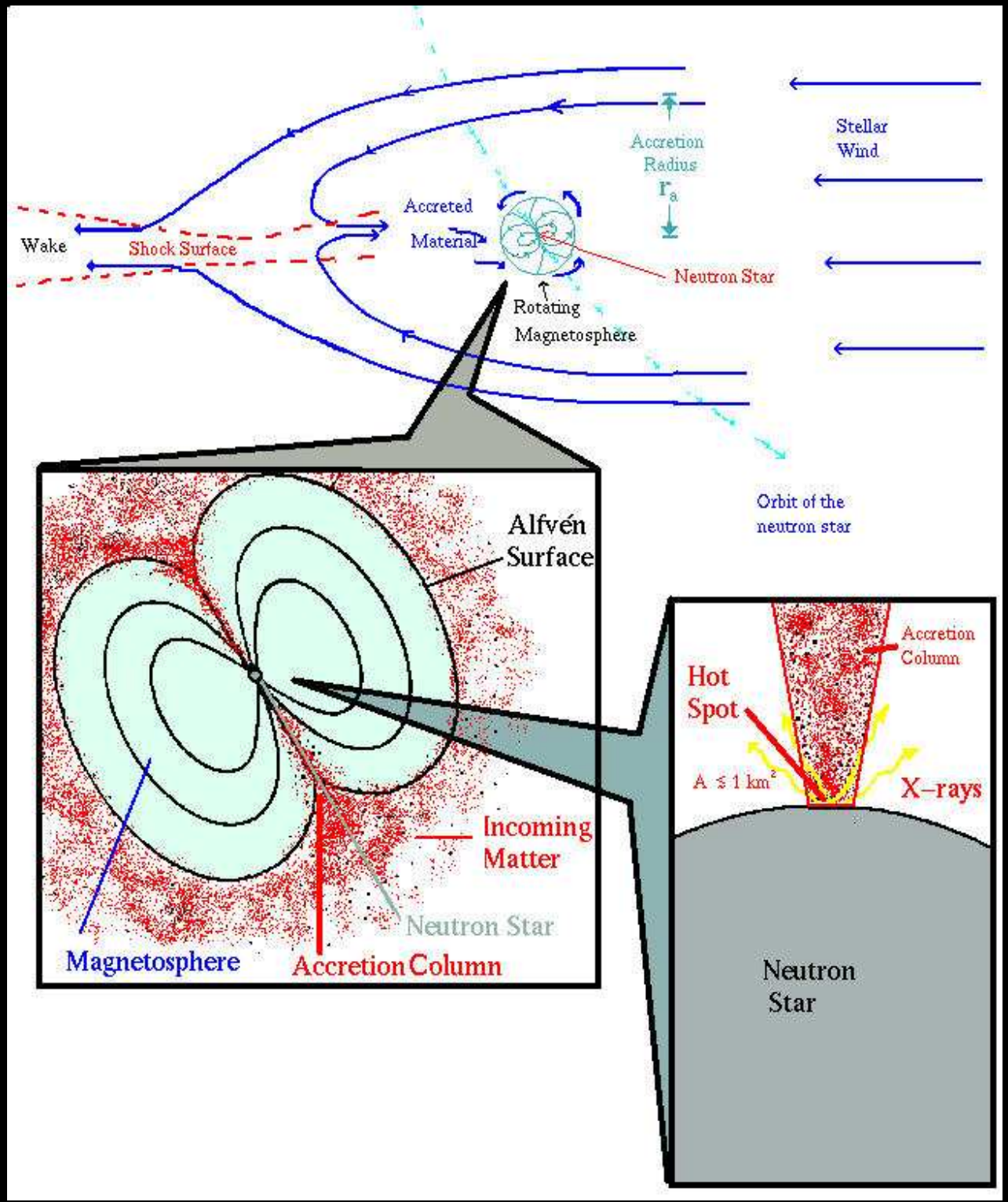

courtesy I. Negueruela, based on Davidson & Ostriker (1973)

Torquing of the Disk

At distance r from the Neutron Star, the Keplerian velocity is

$$v = \sqrt{\frac{GM}{r}} \tag{5.3}$$

and therefore the orbital period ("Kepler period") and frequency are

$$P_{\mathrm{K}} = \frac{2\pi r}{v} = \sqrt{\frac{4\pi^2 r^3}{GM}} \quad \Longleftrightarrow \quad \Omega_{\mathrm{K}} = \frac{2\pi}{P_{\mathrm{K}}} = \sqrt{\frac{GM}{r^3}} \tag{5.4}$$

For $r = 1800\,\mathrm{km}$ and $M = 1.4\,M_\odot$, $P = 1\,\mathrm{s}$.

Since the magnetic field couples the accretion disk to the neutron star, we expect accreting neutron stars to have periods on the order of one second.

. . . provided the coupling between the accretion disk and the B-fi eld is strong enough

Torquing of the Disk

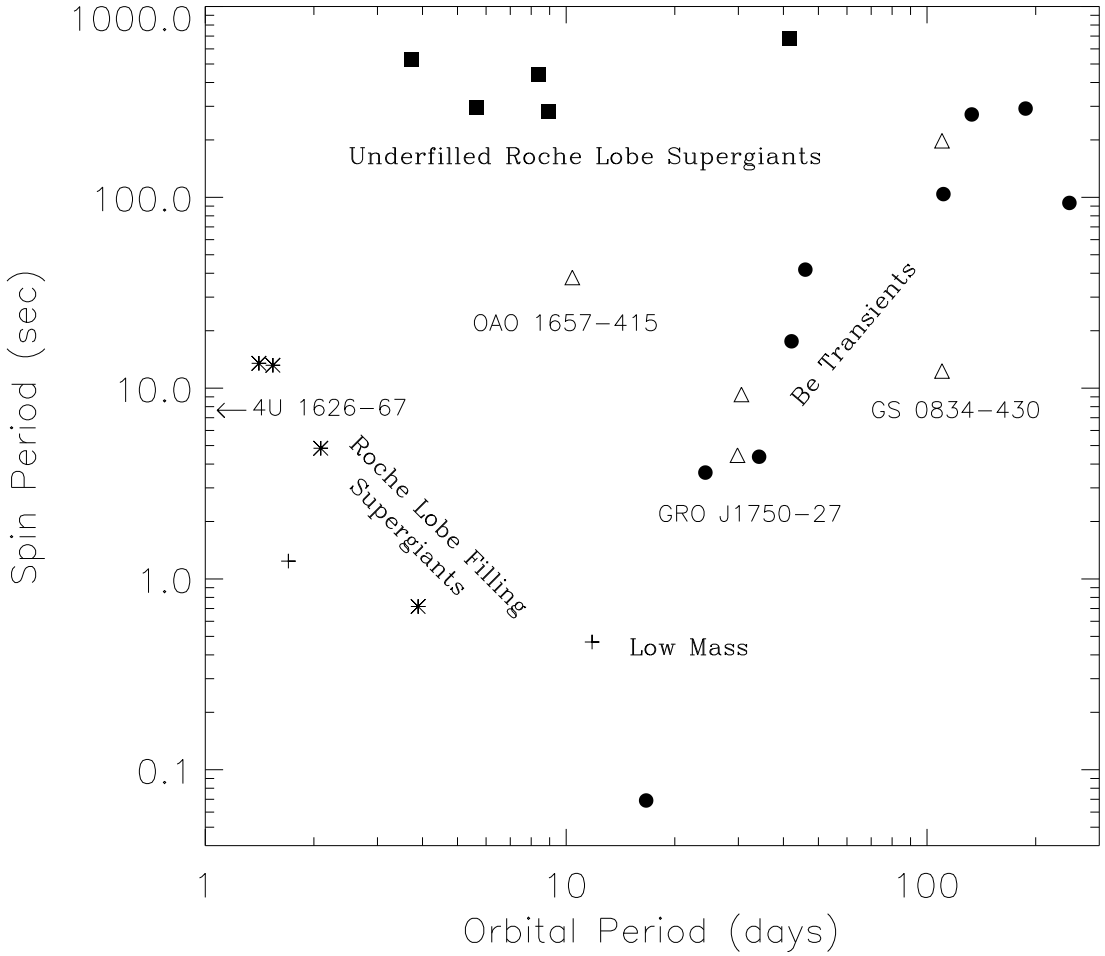

Corbet diagram: Spin period vs. orbital period for HMXB

- Roche lobe overflow: low P_{spin}, low P_{orb}, $L_{\text{X}} \gtrsim 10^{37}\,\text{erg}\,\text{s}^{-1}$
- Wind accretors: longer orbital periods (to avoid Roche lobe overflow), $L_{\text{X}} \sim 10^{35-37}\,\text{erg}\,\text{s}^{-1}$
- Be systems: correlation between spin and orbital periods (higher P_{orb}: less time to torque neutron star?).

Torquing of the Disk

Coupling between magnetic field and accretion disk: accretion disk excerts torque onto NS:

$$I\dot{\omega} = \dot{M} r_{\mathrm{mag}}^2 \Omega_{\mathrm{K}}(r_{\mathrm{mag}}) = \dot{M}\sqrt{GMr_{\mathrm{mag}}} \tag{5.5}$$

where the moment of inertia of the neutron star is $I = (2/5)MR_\star^2$ and where $\Omega_{\mathrm{K}}(r_{\mathrm{mag}})$ is the Kepler frequency at r_{mag} (Eq. 5.4).

Derivation: disk angular momentum: $\mathcal{L} = rmv = r^2 M\Omega$, and therefore the torque is $N = d\mathcal{L}/dt = r^2\dot{M}\Omega$, provided no feedback goes back into the disk.

The luminosity of the source is roughly given as

$$L = \frac{G\dot{M}M}{r_{\mathrm{mag}}} \tag{5.6}$$

After some tedious algebra (Ghosh & Lamb, 1979), one obtains

$$-\frac{\dot{P}}{P} \propto P\, L^{6/7} \tag{5.7}$$

Torquing of the Disk

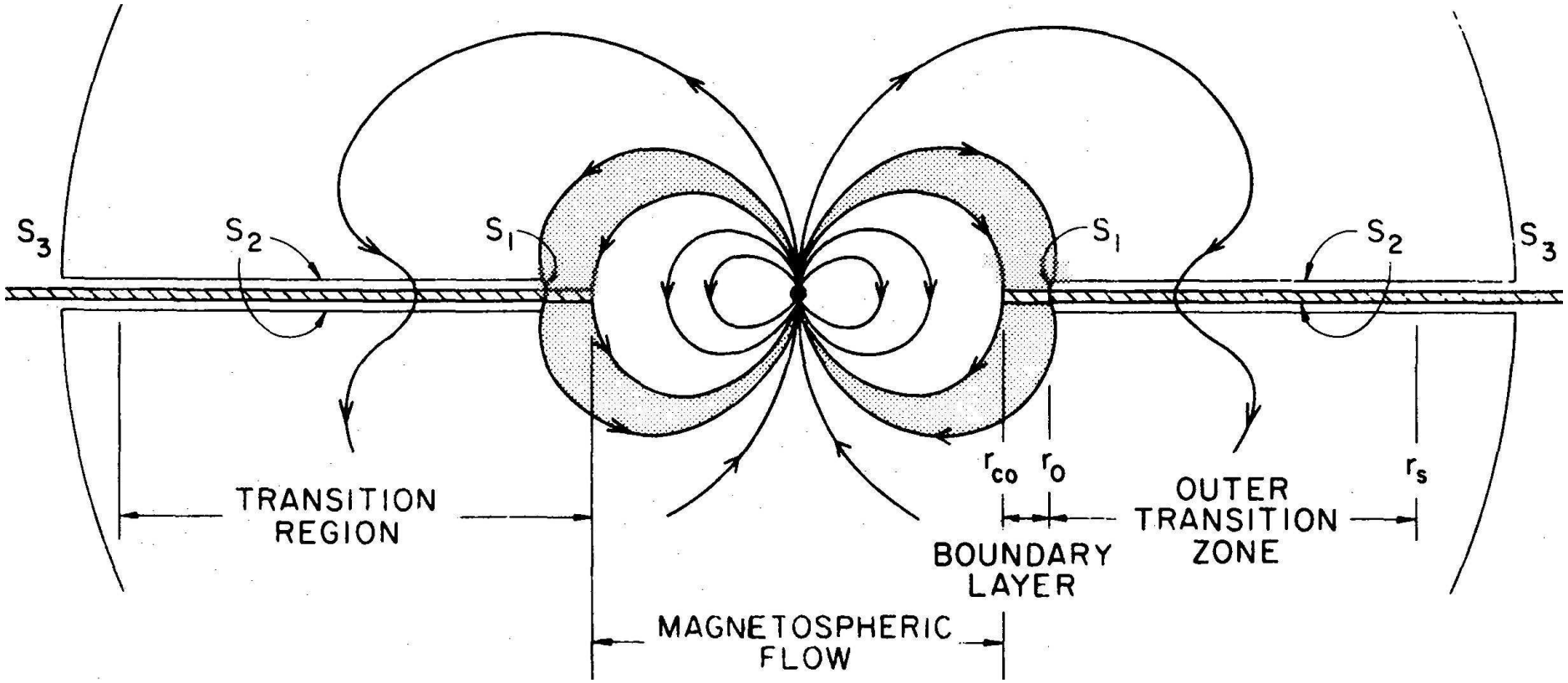

(Ghosh & Lamb, 1979)

In reality the magnetic field is perturbed by the accretion disk

$\Longrightarrow$ calculations get messy

But we'll ignore this. . .

Torquing of the Disk

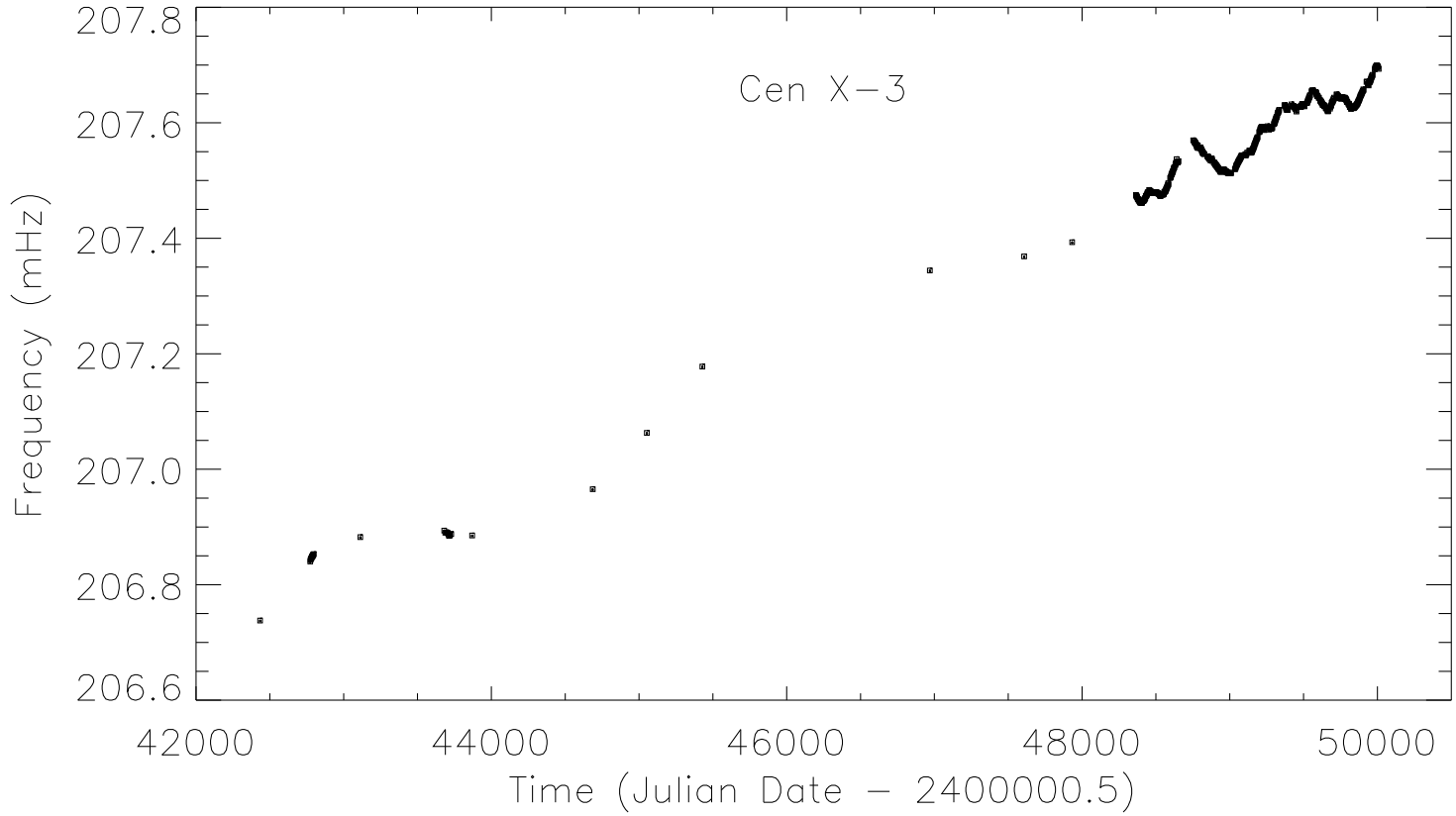

(Bildsten et al., 1997)

Frequency behavior of the HMXB Cen X-3: long-term spin up trend

Spin up: Pulsar becomes faster (i.e., f goes up, resp. P goes down).

Spin down: Pulsar becomes slower (i.e., f goes down, P goes up).

Torquing of the Disk

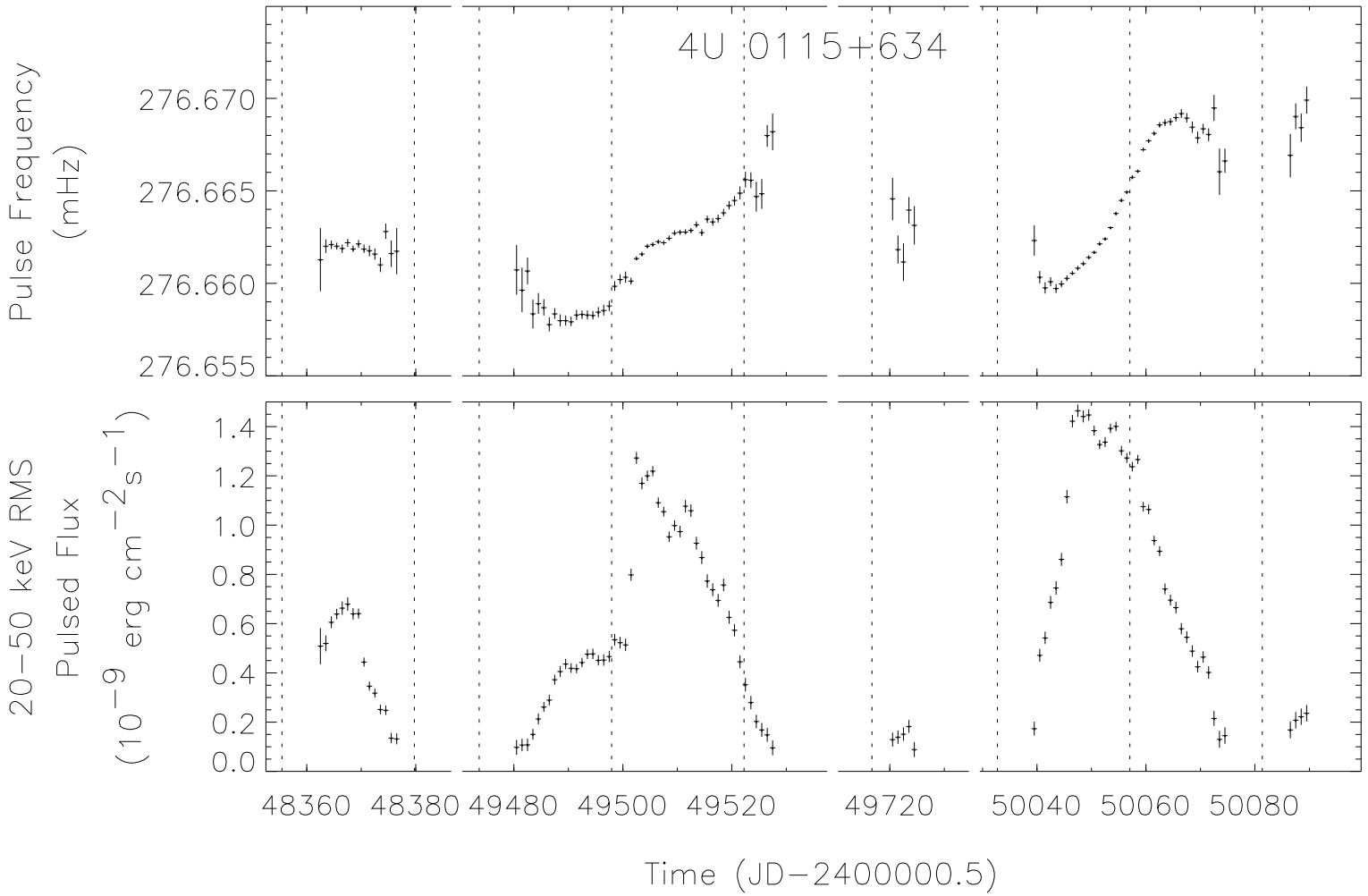

(Bildsten et al., 1997, 4U0115+63 is a Be system, dashed lines are periastron passages)

For transient systems, spin up is correlated with outbursts (i.e., increased $\dot{M}$).

Torquing of the Disk

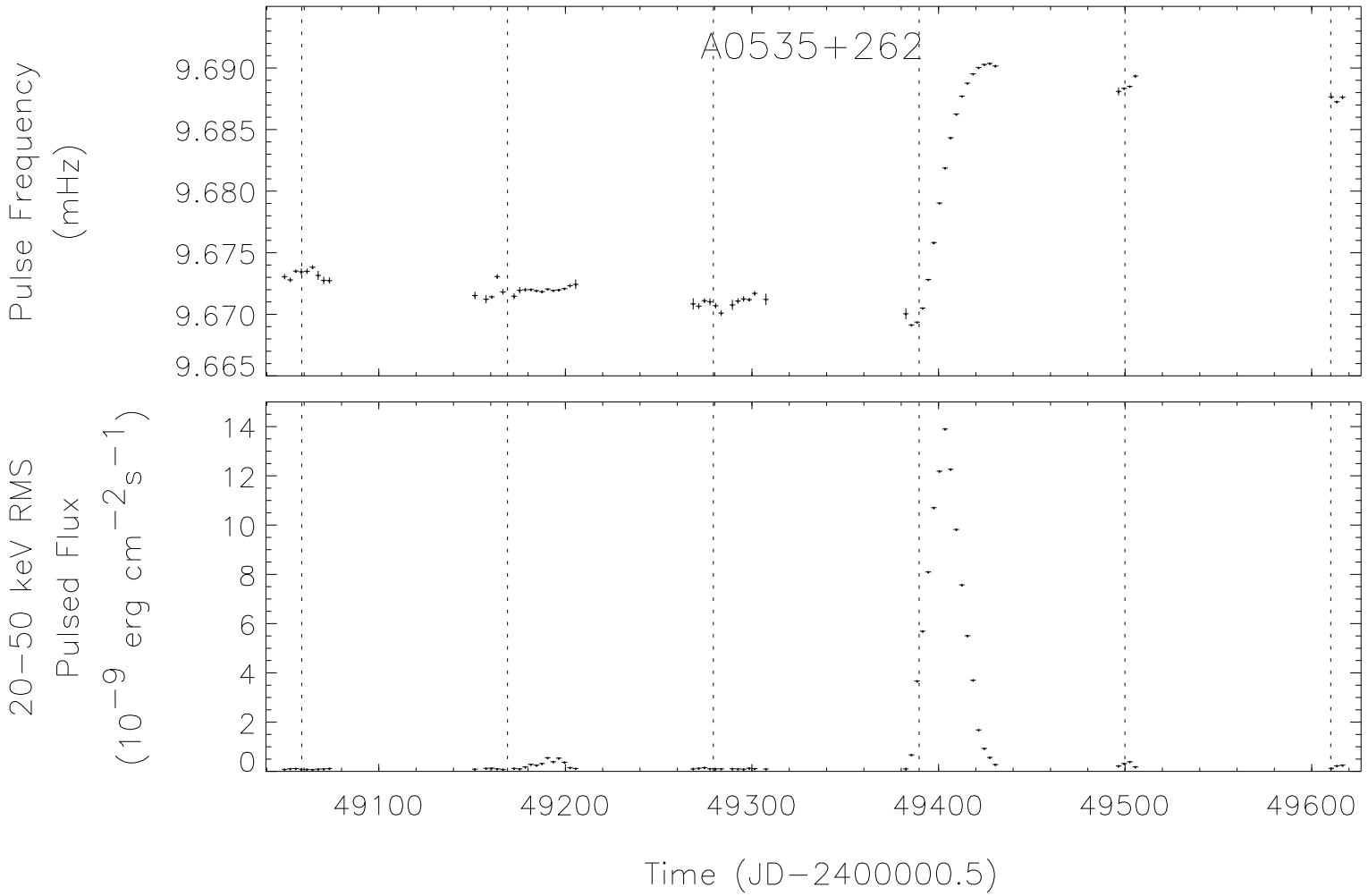

(Bildsten et al., 1997)

For transient systems, spin up is correlated with outbursts (i.e., increased $\dot{M}$).

Torquing of the Disk

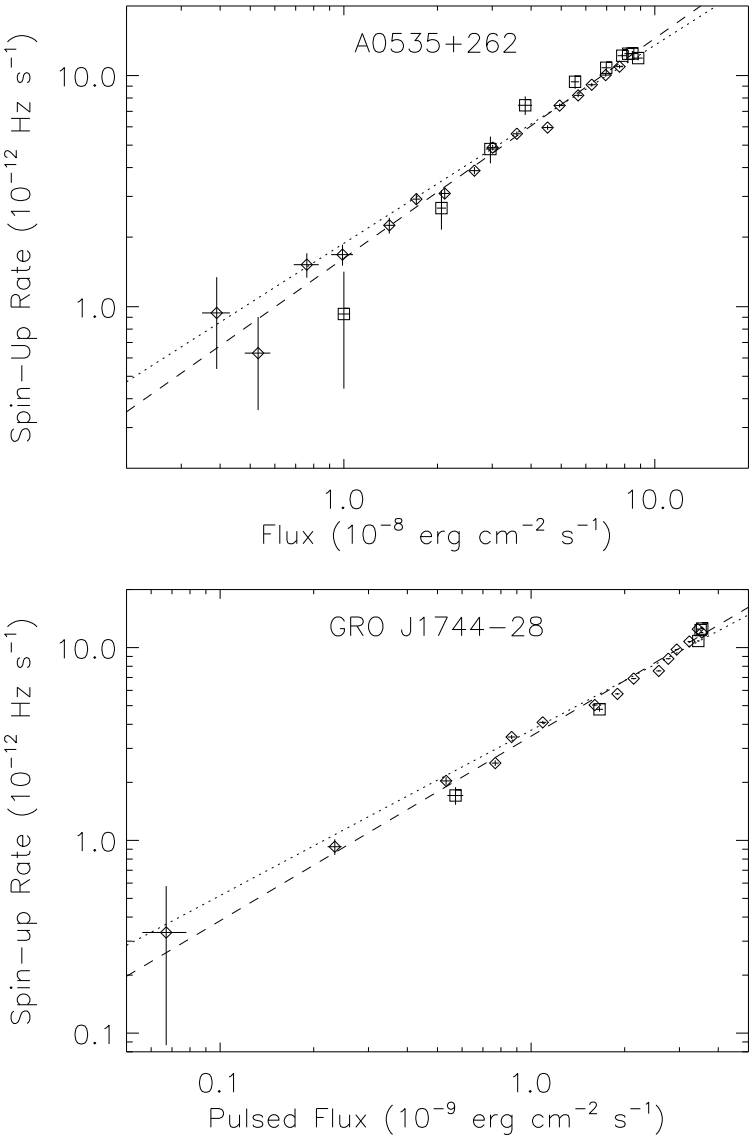

Relationship between $\dot{P}$ and F_X for outbursts of two Be systems.

Dotted: $\dot{P} \propto L^{6/7}$, dashed: best fit power law.

$\Longrightarrow$ Individual outbursts follow torque theory!

more or less, perhaps due to diffi culty in determining bolometric luminosity?

(Bildsten et al., 1997, Fig. 33)

Torquing of the Disk

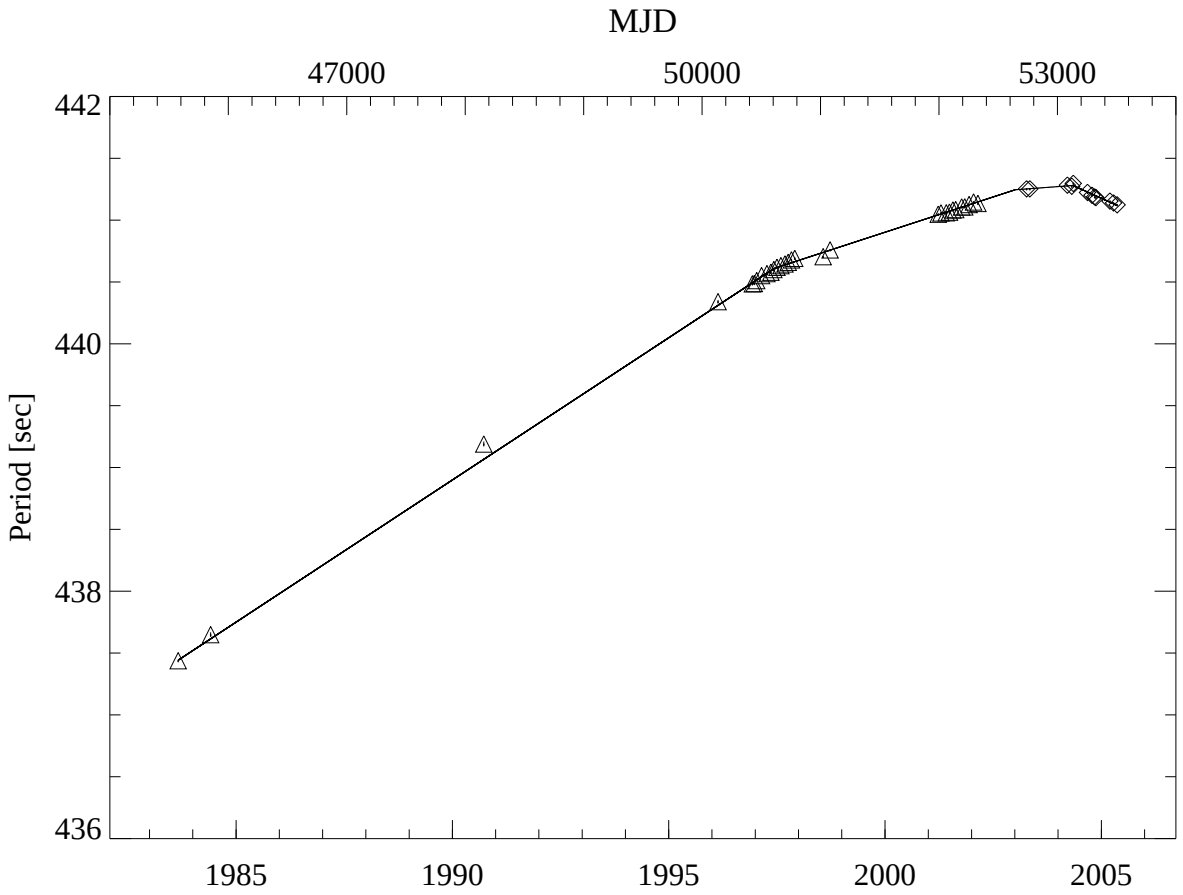

(Fritz et al., 2006)

Not all systems show short term random walk behavior.

4U1907+09: longest continuous spin down in history.

Torquing of the Disk

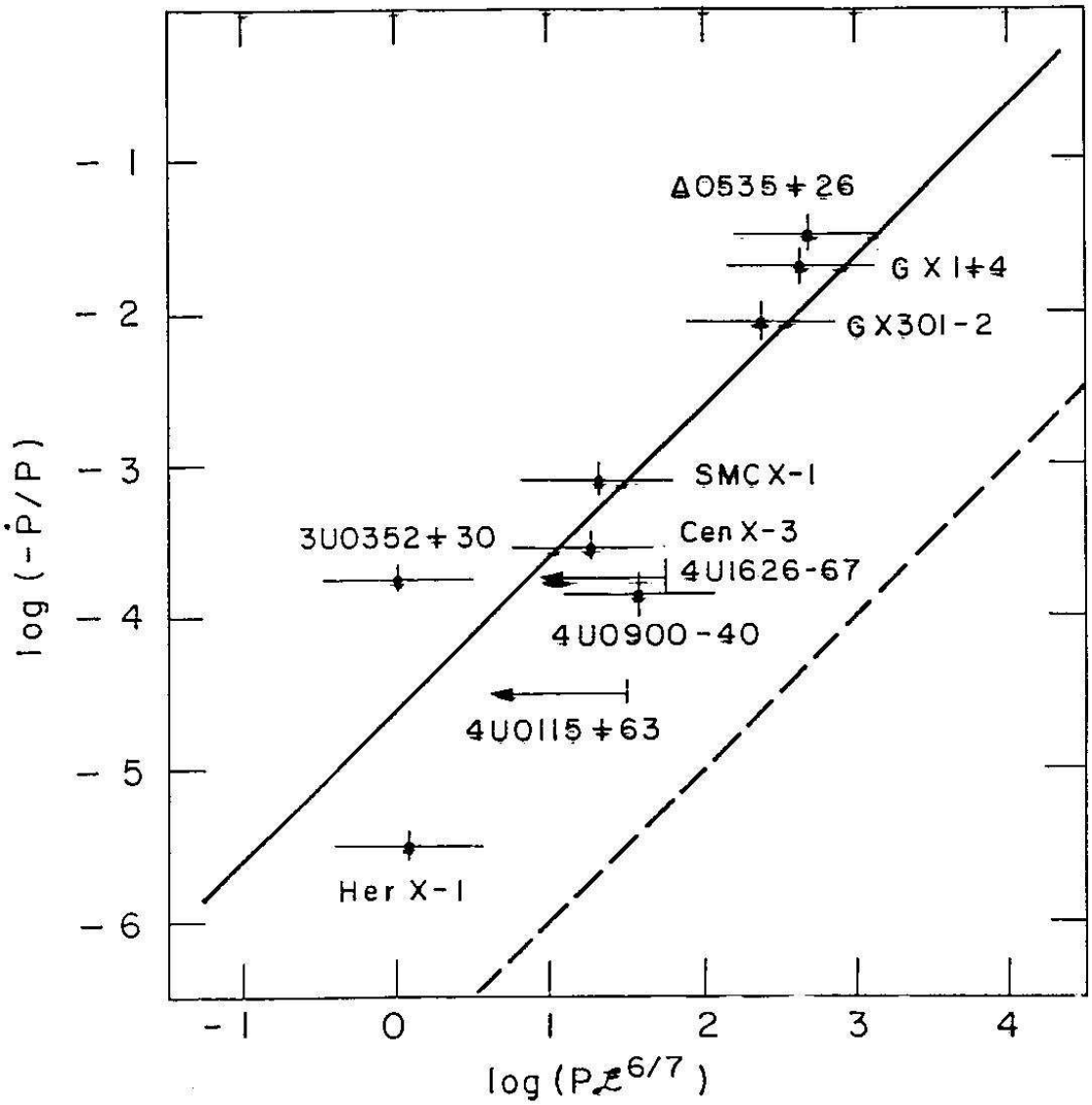

Observations and prediction of magnetospheric accretion model seem to agree.

Note that this works *only* for the long-term trends and outbursts and that there is signifi cant torque jitter superposed to these trends!

(Rappaport & Joss, 1977)

Torquing of the Disk

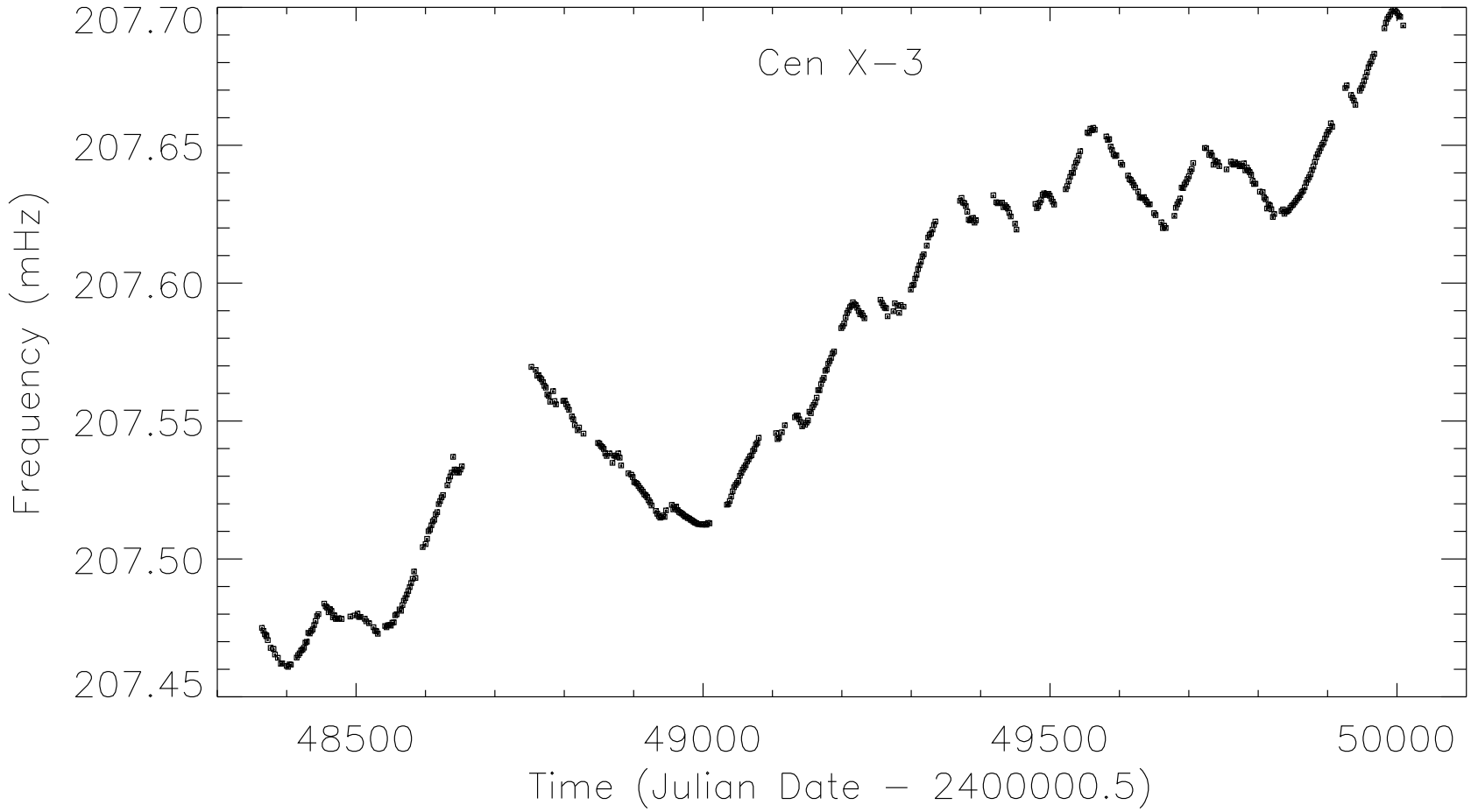

(Bildsten et al., 1997)

Instantaneous torque behavior is very different from long term trends

The Neutron Star Poles: Basic Theory, I

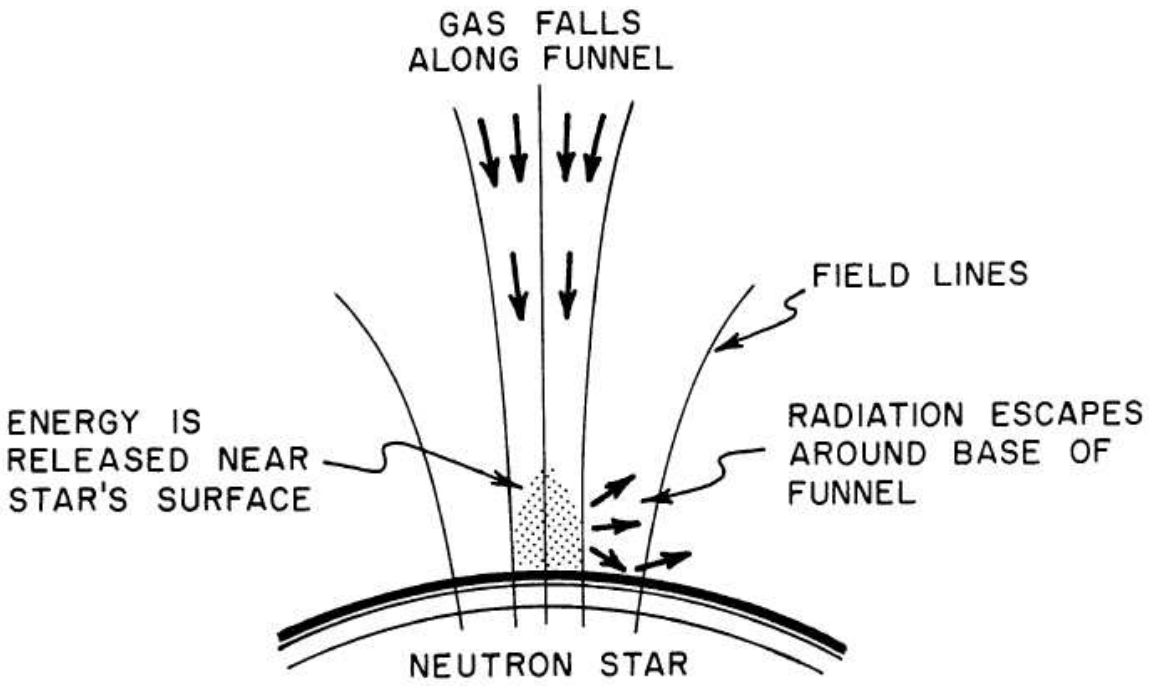

(Ostriker & Davidson, 1973, Fig. 4)

Within $R_{\rm mag}$, low density material

$\Longrightarrow$ approximate free fall along B-field lines.

Speed at magnetic pole:

$$v = \sqrt{\frac{2GM}{R}} \sim 0.65\,c$$

($\sim$140 MeV nucleon^{-1})

The area of the accreting spot is (for a dipolar B-field):

$$\pi r_0^2 = \pi R^2 \cdot (R/r_{\rm mag}) \lesssim 1\,{\rm km}^2$$

see also Pringle & Rees (1972), Gnedin & Sunyaev (1973), and Inoue (1975).

The Neutron Star Poles: Basic Theory, II

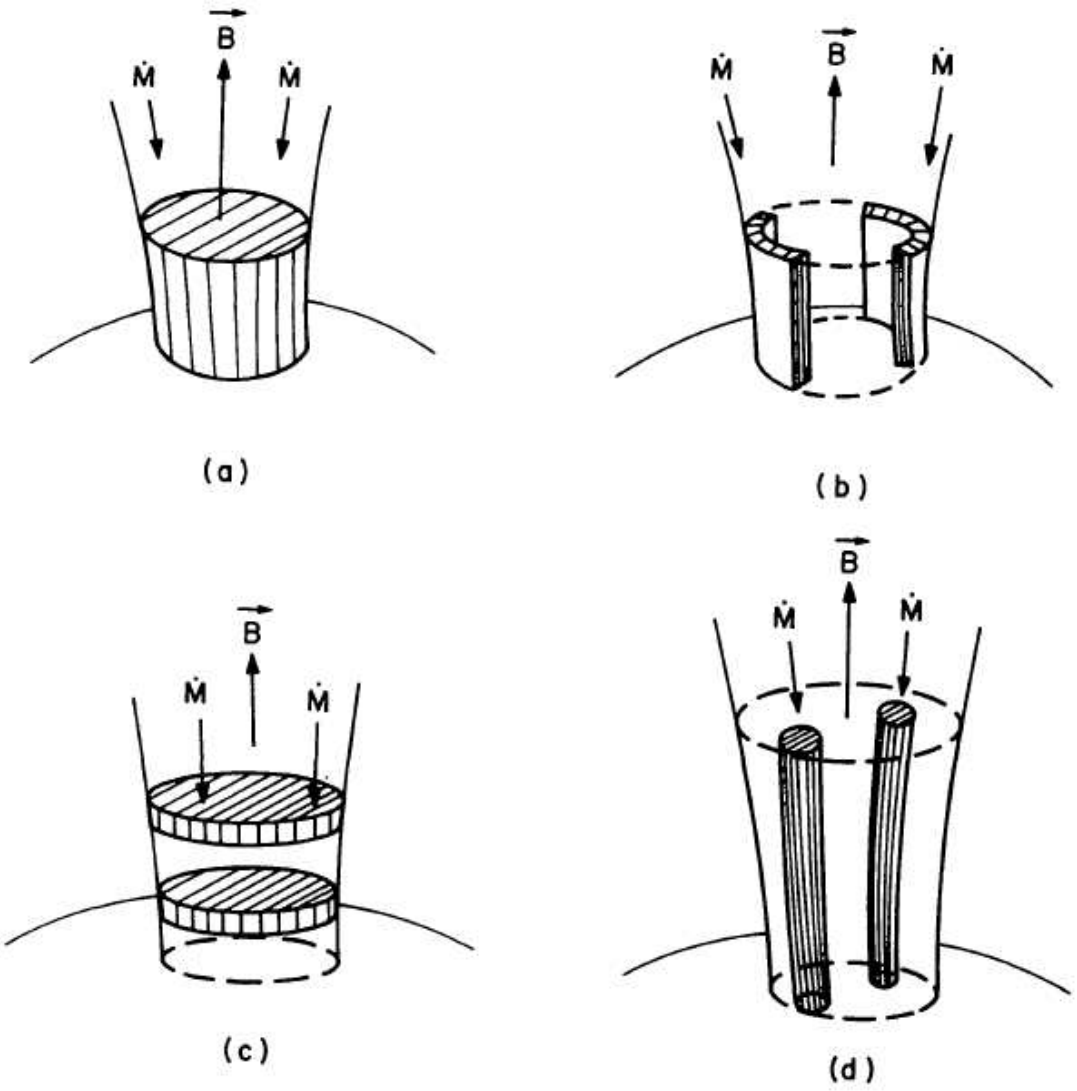

Note: Whether accretion column is filled, a hollow funnel, or “spaghetti like” depends on the details of the coupling of the accretion disk to the B-field, which is not really understood.

(Mészáros, 1984, Fig. 11)

The Neutron Star Poles: Basic Theory, III

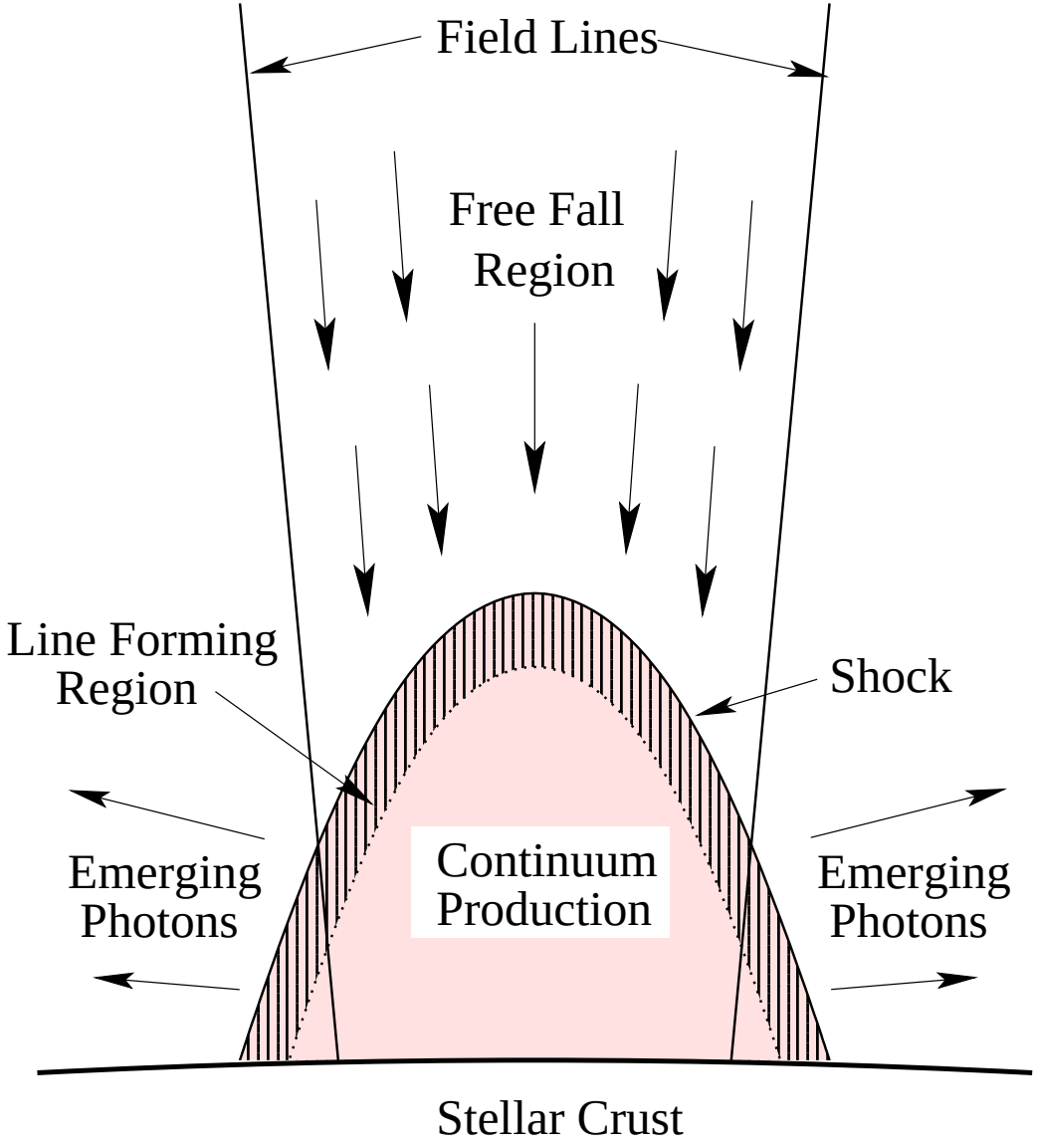

Basic idea of continuum formation:

1. shock $\Longrightarrow$ low energy photons (bremsstrahlung)
2. Compton upscattering in accretion mound/column
3. Photons emerge once $\tau < 1$

Most important process modifying continuum: resonant Compton scattering

(Heindl et al., 2004)

Landau Levels, I

Strong fi eld at neutron star's poles introduces exotic physics:

Quantization of electron energies $\perp B$-fi eld lines (Landau levels):

$$E_n = m_\mathrm{e} c^2 \frac{\sqrt{1 + 2n(B/B_\mathrm{crit}) \sin^2\theta} - 1}{\sin^2\theta} \tag{5.8}$$

$p_\parallel$: momentum of electron $\parallel B$-fi eld, n: major quantum number, B_crit is

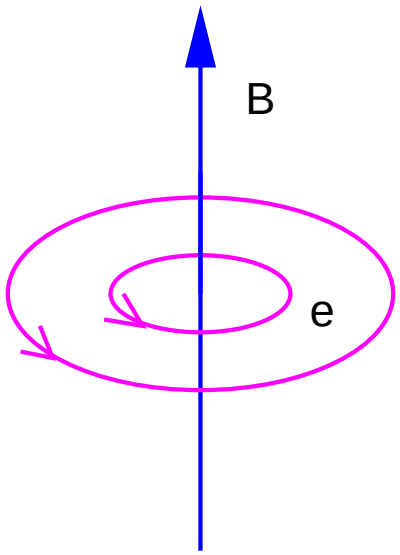

$$B_\mathrm{crit} = \frac{m_\mathrm{e}^2 c^3}{\mathrm{e}\hbar} \sim 4.4 \times 10^{13}\,\mathrm{G} \tag{5.9}$$

For $B \ll B_\mathrm{crit}$, distance between Landau levels:

$$E_\mathrm{cyc} = \frac{\hbar e}{m_\mathrm{e} c} B = 11.6\,\mathrm{keV} \left(\frac{B}{10^{12}\,\mathrm{G}} \right) \tag{5.10}$$

($12 - B_{12}$-rule)

$\Longrightarrow$ Cyclotron Resonance Scattering Features ("Cyclotron lines") at

$$E_n = n E_\mathrm{cyc} = (1 + z) E_{n,\mathrm{obs}} \tag{5.11}$$

($1 + z \sim 1.25 \ldots 1.4$; grav. redshift!)

In the following, a quick derivation of the basic physics of electrons in strong magnetic fi elds is given, followingMészáros (1992). Note that this is rather advanced quantum mechanics, and while you should know the end results, the detailed derivation is beyond the scope of the lecture.

The (relativistic) equation of motion of an electron in a magnetic fi eld is given by

$$\frac{d}{dt}(\gamma m \boldsymbol{v}) = \frac{q}{c}\boldsymbol{v} \times \boldsymbol{B} \tag{5.12}$$

where the Lorentz factor, γ, is

$$\gamma = \frac{1}{\sqrt{1-\beta^2}} = \frac{1}{\sqrt{1-\left(\frac{v}{c}\right)^2}} \tag{5.13}$$

If we ignore the radiative losses caused by the acceleration of the electron, then $\gamma =$ const. and the equation of motion is

$$\frac{d\boldsymbol{v}_{\|}}{dt} = 0 \tag{5.14}$$

$$\gamma m \frac{d\boldsymbol{v}_{\perp}}{dt} = \frac{q}{c}\boldsymbol{v}_{\perp} \times \boldsymbol{B} \tag{5.15}$$

where $\boldsymbol{v}_{\|}$ and $\boldsymbol{v}_{\perp}$ are the components of the velocity vector parallel and perpendicular to the magnetic fi eld, respectively.

Since the force on $\boldsymbol{v}_{\perp}$ is perpendicular to $\boldsymbol{v}_{\perp}$, the motion of the electron will be described by a circular motion around the $\boldsymbol{B}$-fi eld line together with constant motion parallel to the magnetic fi eld.

It is easy to see (check for yourself!) that the frequency of motion around the magnetic fi eld, the so-called *gyrofrequency* is given by

$$\omega_B = \frac{qB}{\gamma mc} = \frac{\omega_{\mathsf{L}}}{\gamma} \tag{5.16}$$

where the *Larmor frequency* is given by

$$\omega_{\mathsf{L}} = \frac{qB}{mc} \tag{5.17}$$

The Larmor frequency is the frequency of a non-relativistically gyrating electron.

Caveat emptor: many authors do not make a distinction between the Larmor frequency and the gyrofrequency. Be careful!

The radius of gyration, the *gyro radius*, is

$$r_g = \gamma v_{\perp} \frac{mc}{qB} = \gamma r_{\mathsf{L}} \tag{5.18}$$

and again, many authors do not distinguish between the gyro radius and the *Larmor radius*.

Finally, the cyclotron energy of the electron is

$$\hbar\omega_g = \hbar\frac{qB}{\gamma mc} \tag{5.19}$$

This classical approach performed so far is valid as long as the Larmor radius is large compared to the de Broglie wavelength of the electron,

$$\lambda_{\mathrm{e}} = \frac{\hbar}{p} = \frac{\hbar}{\gamma m v_\perp} \tag{5.20}$$

Therefore, QM effects are important once

$$\frac{\hbar}{\gamma m v_\perp} \geq \frac{v\gamma mc}{qB} \tag{5.21}$$

that is, for magnetic fi elds

$$B \geq \frac{m^2c^3\gamma^2}{q\hbar}\left(\frac{v_\perp}{c}\right)^2 = \gamma^2\beta_\perp^2\frac{m^2c^3}{e\hbar} = \gamma^2\beta_\perp^2 B_{\mathrm{c}} \tag{5.22}$$

here, $B_{\mathrm{c}} = m^2c^3/(q\hbar) \sim 4.4 \times 10^{13}$ G is the *critical magnetic field*. This name derives from the fact that the nonrelativistic (!!!) cyclotron energy can be written as

$$\hbar\omega_{\mathrm{L}} = mc^2\frac{B}{B_{\mathrm{c}}} \tag{5.23}$$

that is, for $B = B_{\mathrm{c}}$ the nonrelativistic cyclotron energy equals the electron's rest mass. B_{c} is thus a natural quantum mechanical measure for the strength of magnetic fi elds.

Example: For $kT = 10$ keV, $\beta^2 = 5.6 \times 10^{-2}$ and $\gamma \sim 1$, such that for $B \sim 10^{12}$ G quantum mechanics cannot be ignored.

Electrodynamics shows that the generalized momentum for the motion of particles in a magnetic fi eld is

$$\boldsymbol{p} = m\boldsymbol{v} - \frac{e}{c}\boldsymbol{A} \tag{5.24}$$

where $\boldsymbol{A} = \nabla \times \boldsymbol{B}$, and (in the *Landau gauge*)

$$\boldsymbol{A} = \frac{1}{2}\boldsymbol{B} \times \boldsymbol{r} = \frac{1}{2}Br\hat{\varphi} \tag{5.25}$$

where $\hat{\varphi}$ is an unit vector along the azimuthal angle coordinate. The classical equation of motion for these particles is

$$\frac{mv^2}{r} = \frac{qv}{c}B \tag{5.26}$$

and the quantization condition is (similarly to the Bohr atom!)

$$\boldsymbol{p} \times \boldsymbol{r} = n\hbar\hat{B} \tag{5.27}$$

where $\hat{B}$ is an unit vector in the direction of the magnetic fi eld.

Inserting the generalized momentum into the quantization condition gives after some algebra

$$mvr - \frac{1}{2}\frac{eB}{c}r^2 = n\hbar \tag{5.28}$$

After dividing by m and noticing that $v = \omega_g r$ one fi nds

$$\frac{1}{2}\omega_g r^2 = \frac{n\hbar}{m} \tag{5.29}$$

Using Eq. (5.26), the kinetic energy can then be found from

$$E_n = \frac{1}{2}mv^2 = \frac{evB}{2c}r = \frac{1}{2}\frac{eB}{c}\frac{2n\hbar}{m} = n\hbar\omega_g \tag{5.30}$$

Similarly one obtains for the orbital radii

$$r_n = \sqrt{\frac{2n\hbar c}{qB}} = 2.6\text{Å} \cdot \sqrt{\frac{2n}{B_{12}}} \tag{5.31}$$

where $B_{12} = B/10^{12}$ G.

The proper derivation of the Landau levels starts from the Schrödinger equation for the motion of a charged particle in an electromagnetic fi eld. Using again the Landau gauge, the nonrelativistic Hamiltonian is

$$\hat{H} = \frac{1}{2m}\left(\hat{p} - \frac{q}{c}\hat{A}\right)^2 - \frac{q\hbar}{2mc}\hat{\sigma}\cdot\boldsymbol{B} \tag{5.32}$$

where $\hat{\sigma}$ is the Pauli spin operator.

To solve for the wave function ψ, insert the Hamiltonian into the Schrödinger equation

$$\hat{H}\psi = E\psi \tag{5.33}$$

and perform the ansatz

$$\psi = \exp\left(\frac{i}{\hbar}\left(p_x x + p_z z\right)\right)\chi(y) \tag{5.34}$$

After some rather tedious algebra one can then show that the resulting differential equation for χ has the solution

$$E_n = \left(n + \frac{1}{2} + \sigma\right)\hbar\omega_{\text{L}} + \frac{p_z^2}{2m} \tag{5.35}$$

where $\sigma = \pm 1/2$. This is Eq. (5.10). The exact equation, Eq. (5.8) is obtained from solving the Dirac equation in the presence of a magnetic fi eld. This is beyond the scope of this lecture.

Landau Levels, II

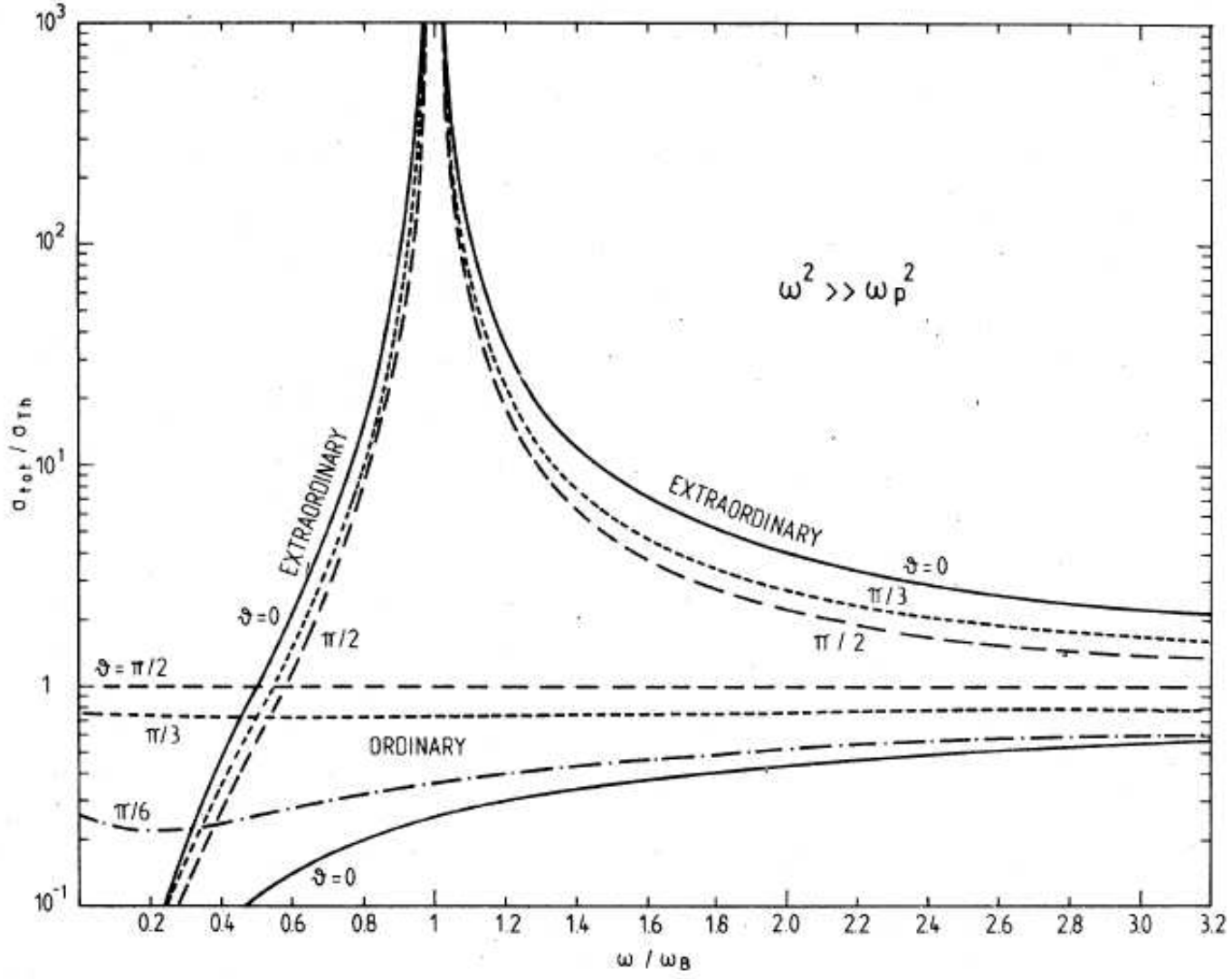

Radiation in accretion column interacts with resonant electrons

$\Longrightarrow$ strong freq. dependence of the scattering cross section

Ventura (1979, Fig. 2), see Gonthier et al. (2000) for good approximations to the cross sections,
and, e.g., Canuto (1970) and Canuto, Lodenquai & Ruderman (1971) for early work.

Accretion Column, I

Interaction of continuum radiation with electrons (Arons, Klein & Lea, 1987):

ordinary mode: E-field of photons in plane spanned by B-field and propagation direction. Continuum process only!

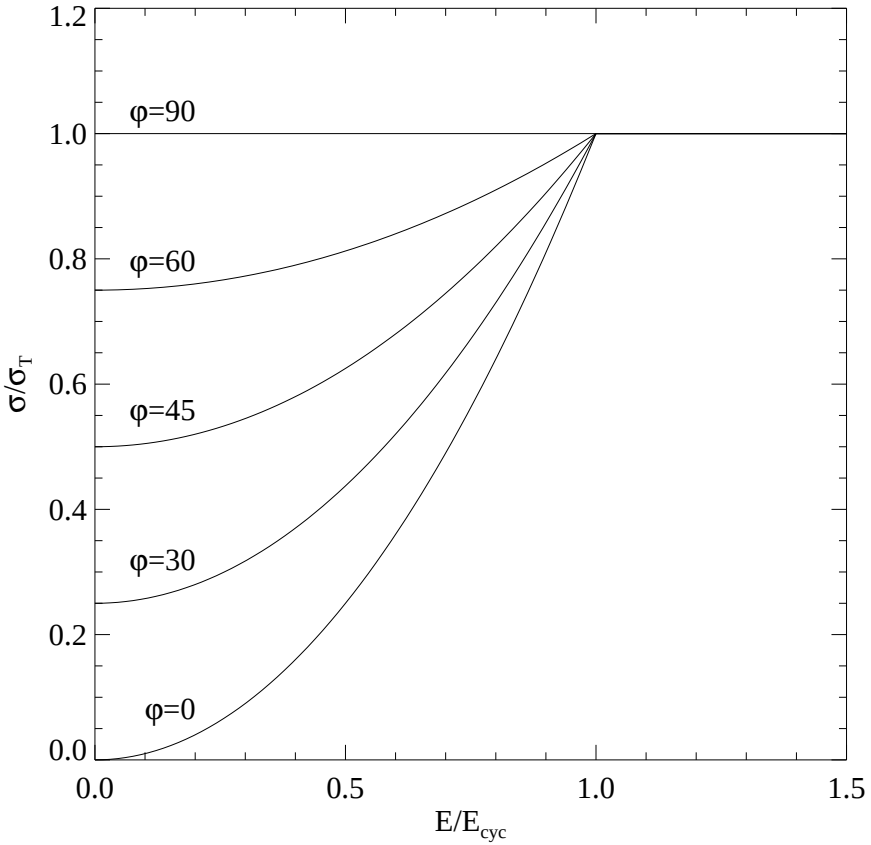

Cross section:

$$\sigma_{\mathrm{ord}}(\varphi) = \sigma_{\mathrm{T}} \left(\sin^2 \varphi + k(\epsilon) \cos^2 \varphi \right)$$

where

$$k(\epsilon) = \begin{cases} 1 & \text{for } E > E_{\mathrm{cyc}} \\ (E/E_{\mathrm{cyc}})^2 & \text{for } E \leq E_{\mathrm{cyc}} \end{cases}$$

where $\sigma_{\mathrm{T}} = 6.65 \times 10^{-25}\,\mathrm{cm}^2$ is the Thomson cross section, and where $\phi = \angle(\boldsymbol{B}, \text{dir. propagation})$.

(using notation of Becker & Wolff, 2007)

Accretion Column, II

extraordinary mode: E-field of photons perpendicular to plane spanned by B-field and direction of propagation.

Continuum *and* resonant scattering possible.

Cross section:

$$\sigma_{\mathrm{ext}}(\varphi) = \sigma_{\mathrm{T}} k(\epsilon) + \sigma_\ell \phi_\ell(E, E_{\mathrm{cyc}}, \varphi)$$

where

- σ_ℓ: resonant cross section,

$$\sigma_\ell \sim 1.9 \times 10^4 \, \frac{\sigma_{\mathrm{T}}}{B_{12}}$$

- $\phi_\ell(E, E_{\mathrm{cyc}}, \varphi)$: line profile

  ($\sim$ Gaussian if taking thermal broadening into account)

Accretion Column, III

Approximate cross sections outside of resonance:

Mode averaged cross section $\parallel \boldsymbol{B}$ ($\varphi = 0°$):

$$\sigma_{\parallel} = \frac{1}{2}\left(\sigma_{\mathrm{ord}}(0°) + \sigma_{\mathrm{ext}}(0°)\right) \sim \sigma_{\mathrm{T}} \left(\frac{E}{E_{\mathrm{cyc}}}\right)^2$$

Mode averaged cross section $\perp \boldsymbol{B}$ ($\varphi = 90°$):

$$\sigma_{\perp} = \frac{1}{2}\left(\sigma_{\mathrm{ord}}(90°) + \sigma_{\mathrm{ext}}(90°)\right) = \sigma_{\mathrm{T}} + \sigma_{\mathrm{T}} \left(\frac{E}{E_{\mathrm{cyc}}}\right)^2 \sim \sigma_{\mathrm{T}}$$

Plasma is much more transparent parallel to the B-field than perpendicular to the B-field!

For order of magnitude estimates, use mean energy of radiation fi eld, $\langle E \rangle$, instead of E in above equations.

Accretion Column, IV

Basko & Sunyaev (1976): Radiation pressure becomes important once

$$L_{\mathrm{X}} \sim L_{\mathrm{crit}} = 2.72 \times 10^{37}\,\mathrm{erg\,s^{-1}}\,\frac{\sigma_{\mathrm{T}}}{\sqrt{\sigma_\perp \sigma_\parallel}}\left(\frac{M}{M_\odot}\right)\left(\frac{r_0}{R}\right)$$

For $L_{\mathrm{X}} \gtrsim L_{\mathrm{crit}}$ flow is super-Eddington and radiation pressure $\gg$ gas pressure.

$\Longrightarrow$ radiation pressure dominated shock

("accreted matter acts as test particles").

implies continuous velocity transition over few Thomson lengths, different from traditional hydrodynamical shocks!

For $L_{\mathrm{X}} \lesssim L_{\mathrm{crit}}$: breaking of plasma by hydrodynamical shock, "Coulomb friction", or nuclear collisions (stopping length $\sim$30–60 g cm^{-2}).

see, e.g., Basko & Sunyaev (1976), Langer & Rappaport (1982), Braun & Yahel (1984)

What physical process is the most important is still very much debated.

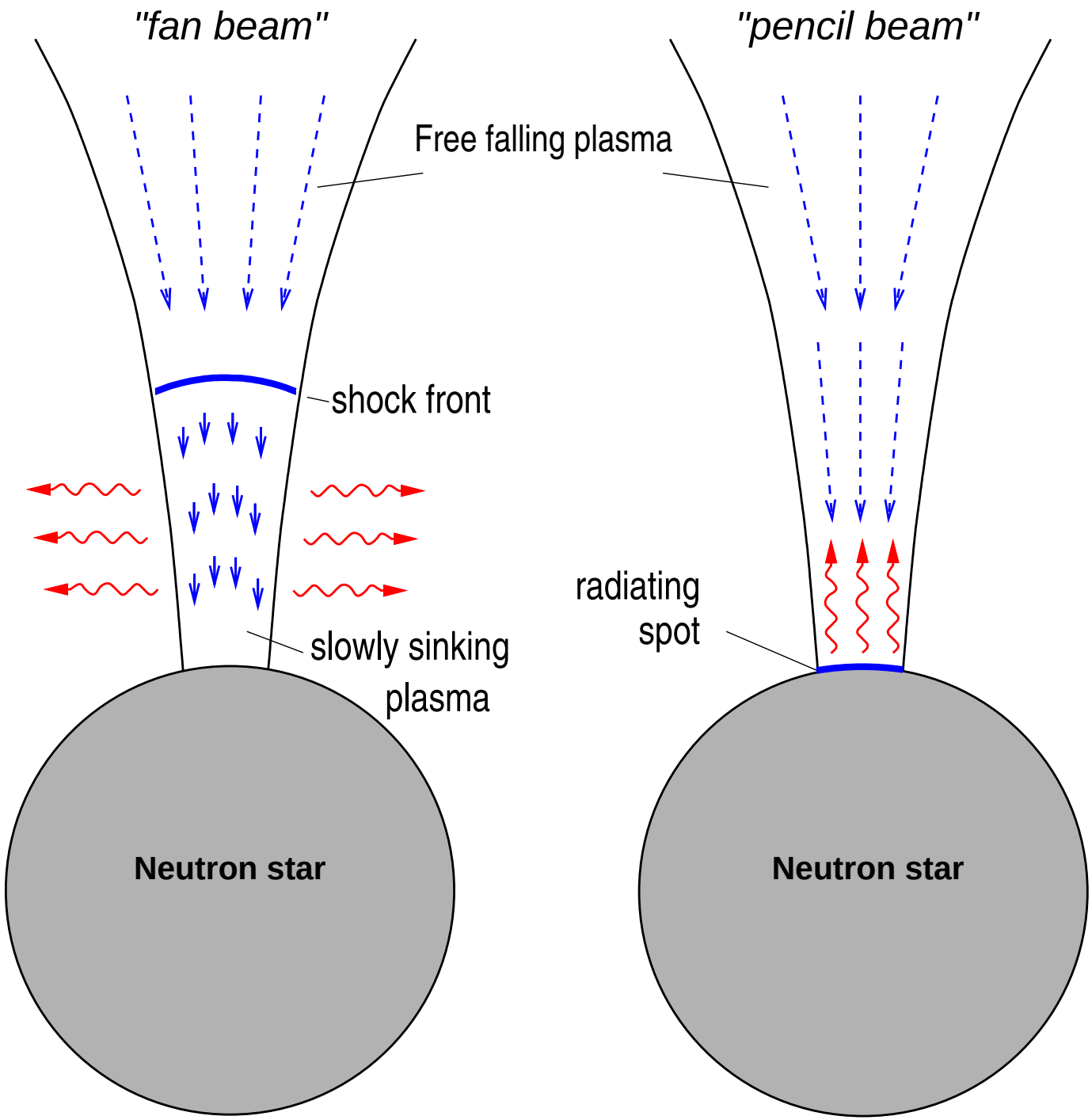

(Kretschmar 1996, Dissertation AIT, Abb. 2.9 [after Harding 1994])

$\Longrightarrow$ “cylinder” and “slab geometries”

Pulse Profi les, I

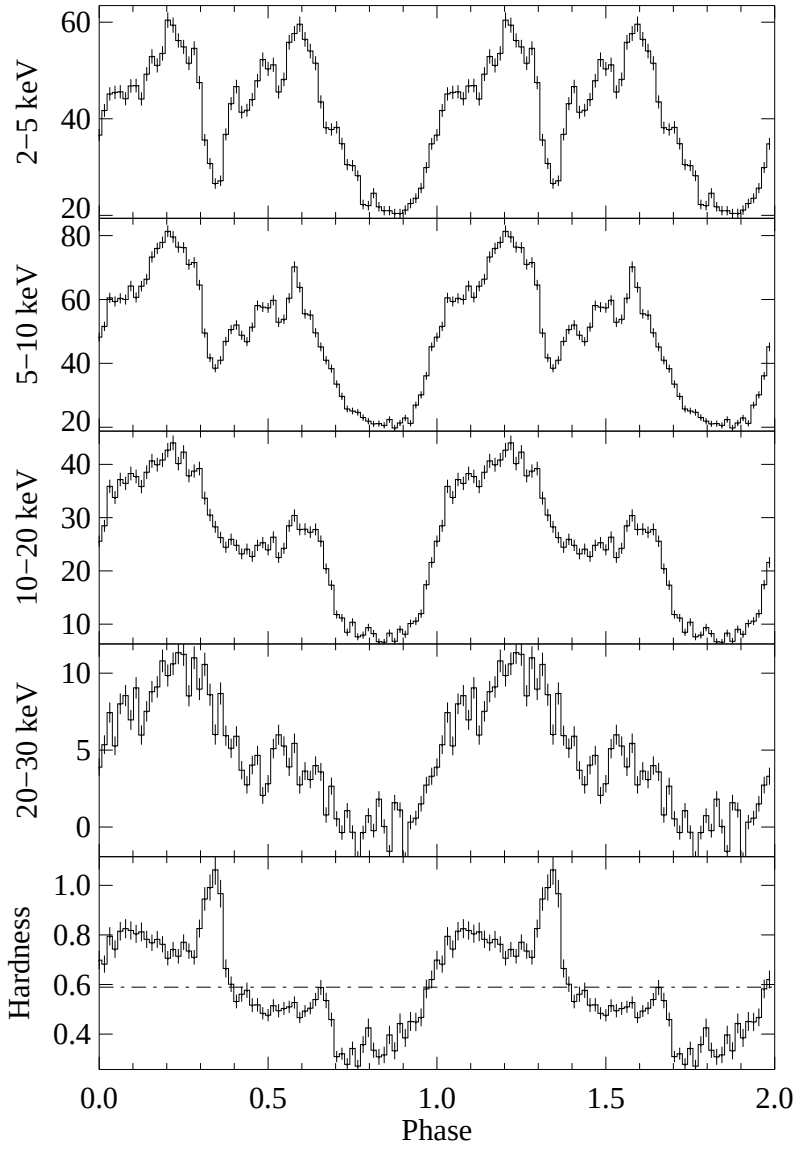

Rotation of accreting neutron star leads to X-ray pulsations.

Typically complex profi les at low E, ∼sinusoidal profi les at higher energies $\Longrightarrow$ due to emission characteristics and absorption in accretion fbw?

Cep X-4 (McBride, et al., submitted)

Pulse Profi les, I

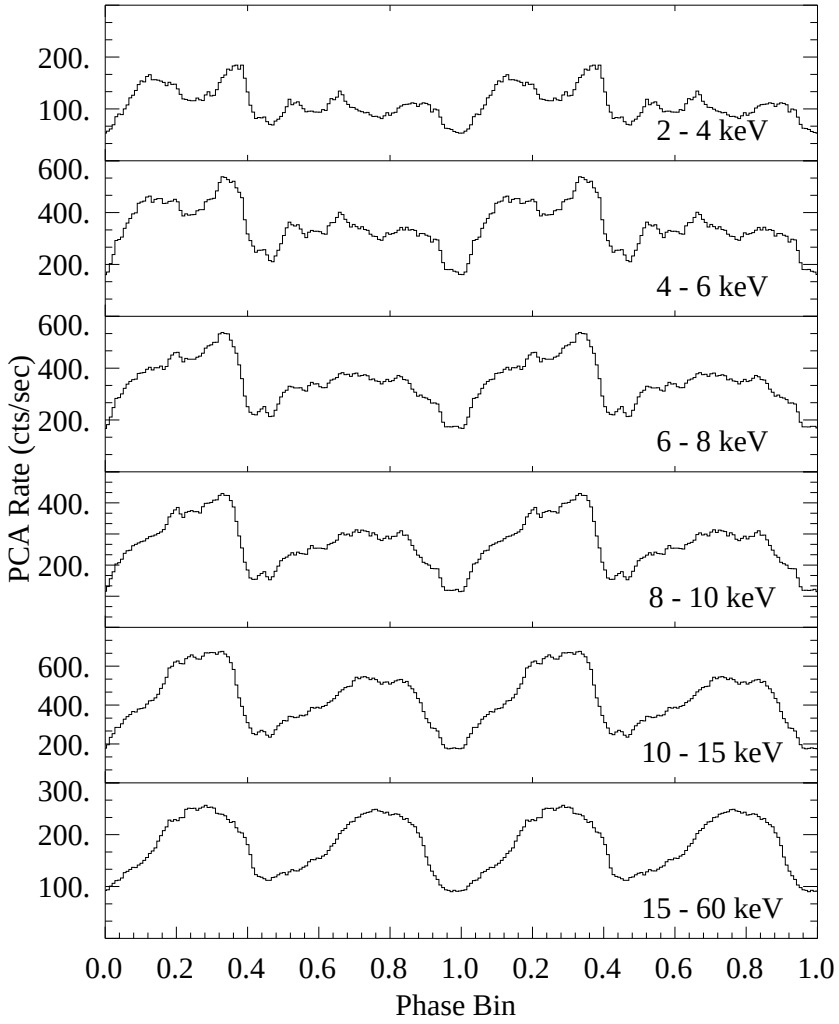

Rotation of accreting neutron star leads to X-ray pulsations.

Typically complex profi les at low E, $\sim$sinusoidal profi les at higher energies $\Longrightarrow$ due to emission characteristics and absorption in accretion fbw?

(Kreykenbohm et al., 1999, Vela X-1)

Pulse Profi les, III

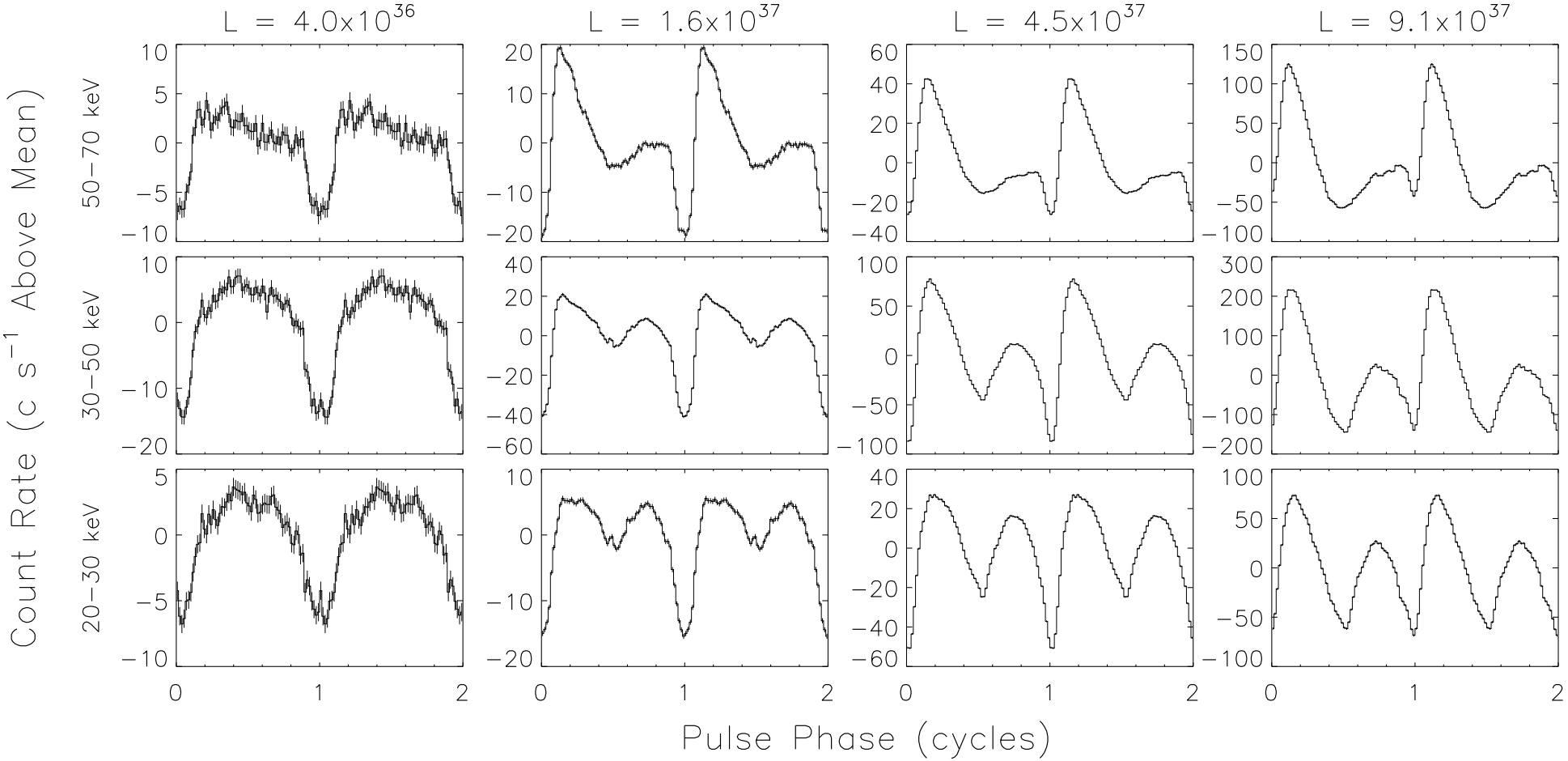

(Bildsten et al., 1997, A0535+35)

Luminosity dependence of the pulse profile of A0535+35 over one outburst.

Spectral Shape

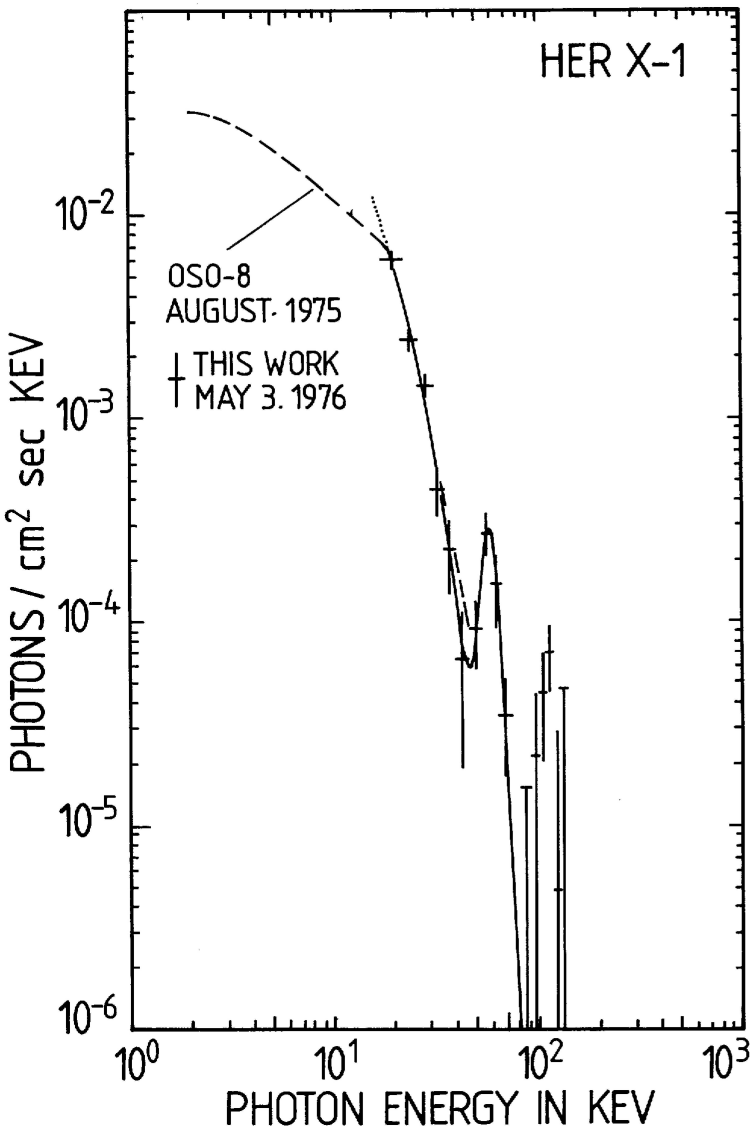

X-ray spectral shape:

- power law continuum with exponential cutoff

  Due to Compton scattering?

- normally strong Fe Kα line at 6.4...6.7 keV

  Due to fluorescence in circumstellar material.

- Cyclotron line due to strong B-field

Her X-1 (Trümper et al., 1978)

Continuum Formation: Early Work

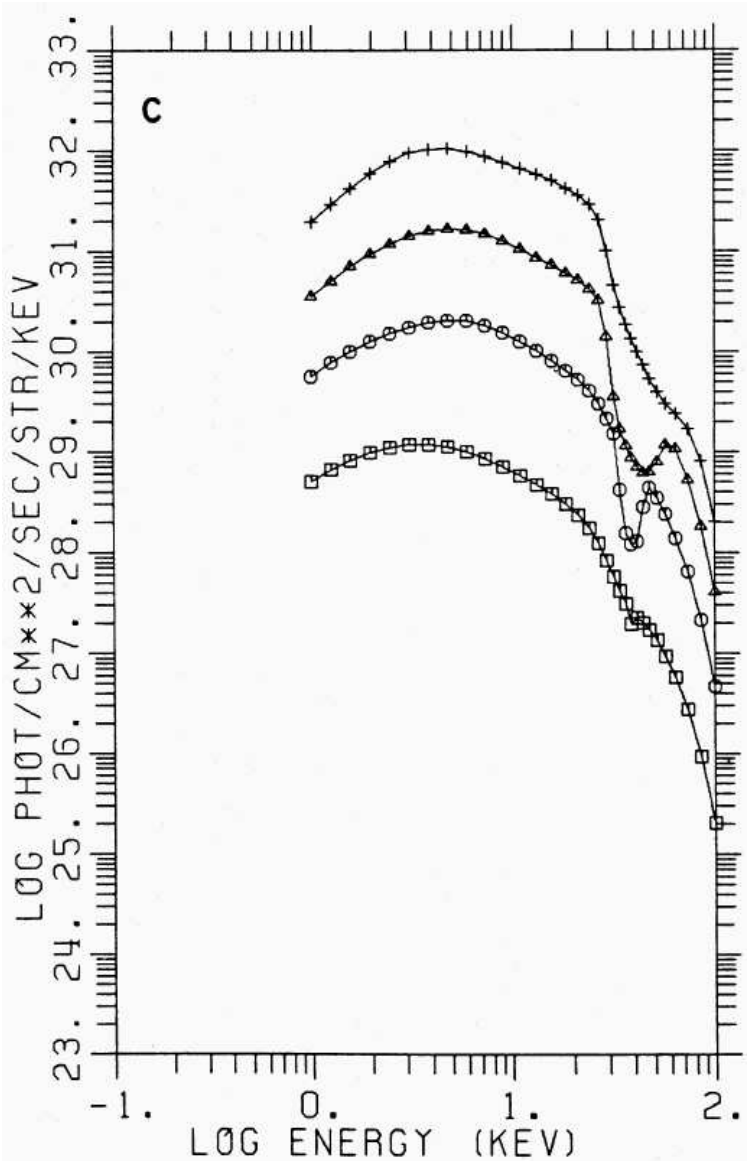

First simple models for accretion column by Nagel (1981a,b) used simplified radiative transfer (“two stream approximation”).

Mészáros & Nagel (1985a,b): angle dependent calculations based on Feautrier methods.

get continua $\sim$ right (about one order of magnitude)

Spectra emerging from a slab (top to bottom $\theta = 21°$, $48°$, $71°$, and $86°$; Mészáros & Nagel 1985a, Fig. 3c)

Continuum Formation: State of the Art

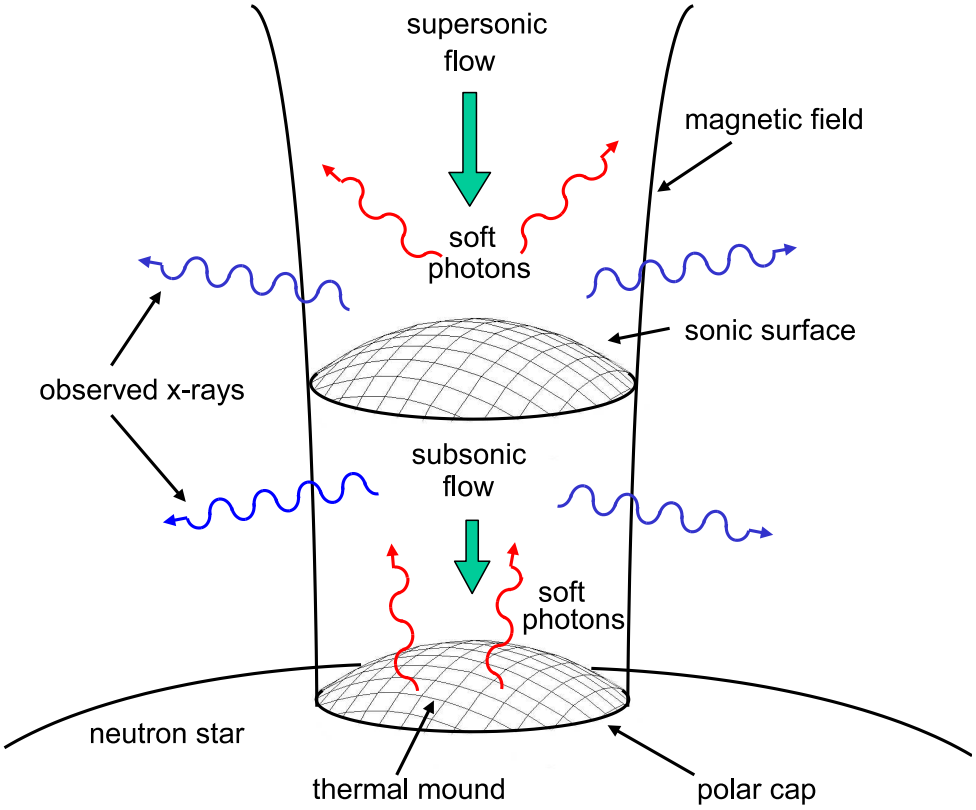

Becker & Wolff (2005a,b, 2007):

Previous work ignores accretion shock.

New picture: bulk motion Comptonization

- accretion mound produces soft X-rays
- X-rays are upscattered in accretion shock
- hard X-rays diffuse through walls of accretion column

Continuum Formation: State of the Art

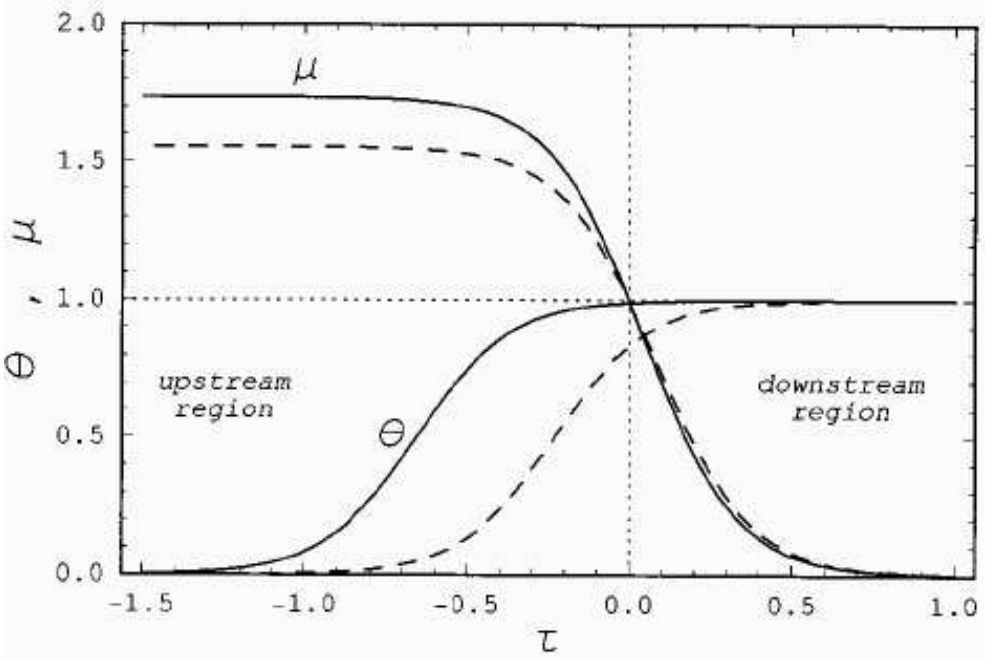

(Becker, 1998, Fig. 2)

Velocity structure of column (Becker, 1998):

$$\beta = \frac{v(x)}{v_c} = \frac{7}{4}\left(1 - \left(\frac{7}{3}\right)^{-1+x/x_{\rm st}}\right)$$

where

- x: distance into column
- $x_{\rm st}$: distance of sonic point from NS surface,

$$x_{\rm st} = \frac{r_0}{2\sqrt{3}}\left(\frac{\sigma_\perp}{\sigma_\parallel}\right)^{1/2} \ln\left(\frac{7}{3}\right)$$

- v_c: sonic point velocity,

$$v_c = \frac{4}{7}\left(\frac{2GM}{R}\right)^{1/2} \sim 0.37c$$

(for typical neutron star parameters)

Continuum Formation: State of the Art

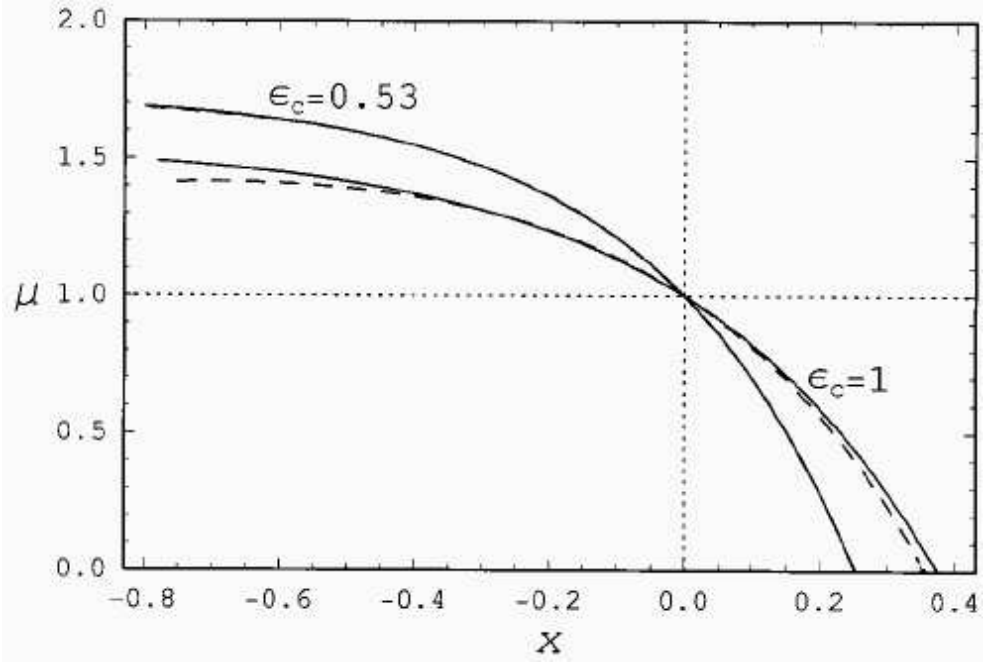

(Becker, 1998, Fig. 9)

Velocity structure of column (Becker, 1998):

$$\beta = \frac{v(x)}{v_c} = \frac{7}{4}\left(1 - \left(\frac{7}{3}\right)^{-1+x/x_{\rm st}}\right)$$

where

- x: distance into column
- $x_{\rm st}$: distance of sonic point from NS surface,

$$x_{\rm st} = \frac{r_0}{2\sqrt{3}}\left(\frac{\sigma_\perp}{\sigma_\parallel}\right)^{1/2} \ln\left(\frac{7}{3}\right)$$

- v_c: sonic point velocity,

$$v_c = \frac{4}{7}\left(\frac{2GM}{R}\right)^{1/2} \sim 0.37c$$

(for typical neutron star parameters)

Continuum Formation: State of the Art

Mathematical implementation of the model: calculate Green's function, f_{G}, for response of column:

$$v\frac{\partial f_{\mathsf{G}}}{\partial x} = \frac{dv}{dx}\frac{\epsilon}{3}\frac{\partial f_{\mathsf{G}}}{\partial \epsilon}$$ bulk Comptonization (1st order Fermi)

$$+ \frac{\partial}{\partial x}\left(\frac{c}{3n_{\mathsf{e}}\sigma_{\parallel}}\frac{\partial f_{\mathsf{G}}}{\partial x}\right)$$ spatial diffusion in x-direction ($\parallel$ column axis)

$$- \frac{f_{\mathsf{G}}}{t_{\mathsf{esc}}}$$ escape from the column

$$+ \frac{\dot{N}_0\delta(\epsilon-\epsilon_0)\delta(x-x_0)}{\pi r_0^2\epsilon_0^2}$$ photon injection

$$- \beta v_0 f_{\mathsf{G}}\delta(x-x_0)$$ absorption in the thermal mound

where

- ϵ: photon energy
- n_{e}: electron number density
- $v_0 = v(x_0)$: flow velocity at source location x_0
- $\epsilon^2 f_0 d\epsilon$: photon number density at x_0
- β: absorptivity of the mound, determined self-consistently

Continuum Formation: State of the Art

Becker & Wolff (2005a,b): bulk Comptonization only (via Kompaneets equation, i.e., no Compton recoil)

$\Longrightarrow$ no cutoff, $\Gamma \geq 2$

This limitation has been removed by Becker & Wolff (2007).

Physical processes for scattering:

- bulk Comptonization
- thermal Comptonization

(via Kompaneets equation).

Seed photons:

- bremsstrahlung (from within column)
- cyclotron radiation (from within column)
- black body radiation (from bottom of column)

Continuum Formation: State of the Art

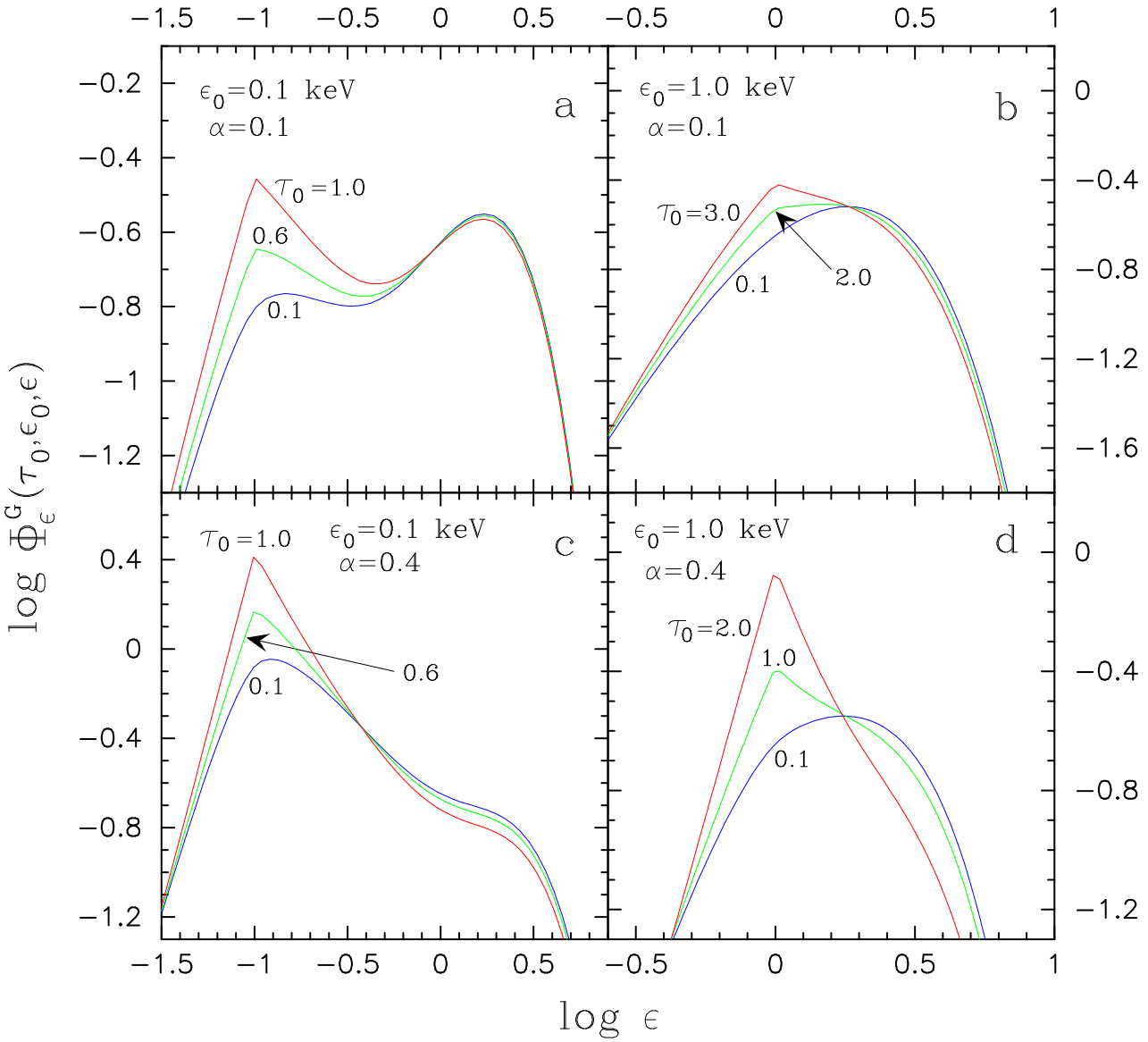

Column integrated Green's functions as a function of energy and optical depth.

(assuming $\sigma_{\parallel} = 10^{-3}\,\sigma_T$, $\sigma_{\perp} = \sigma_T$).

(Becker & Wolff, 2007, Fig. 3)

Continuum Formation: State of the Art

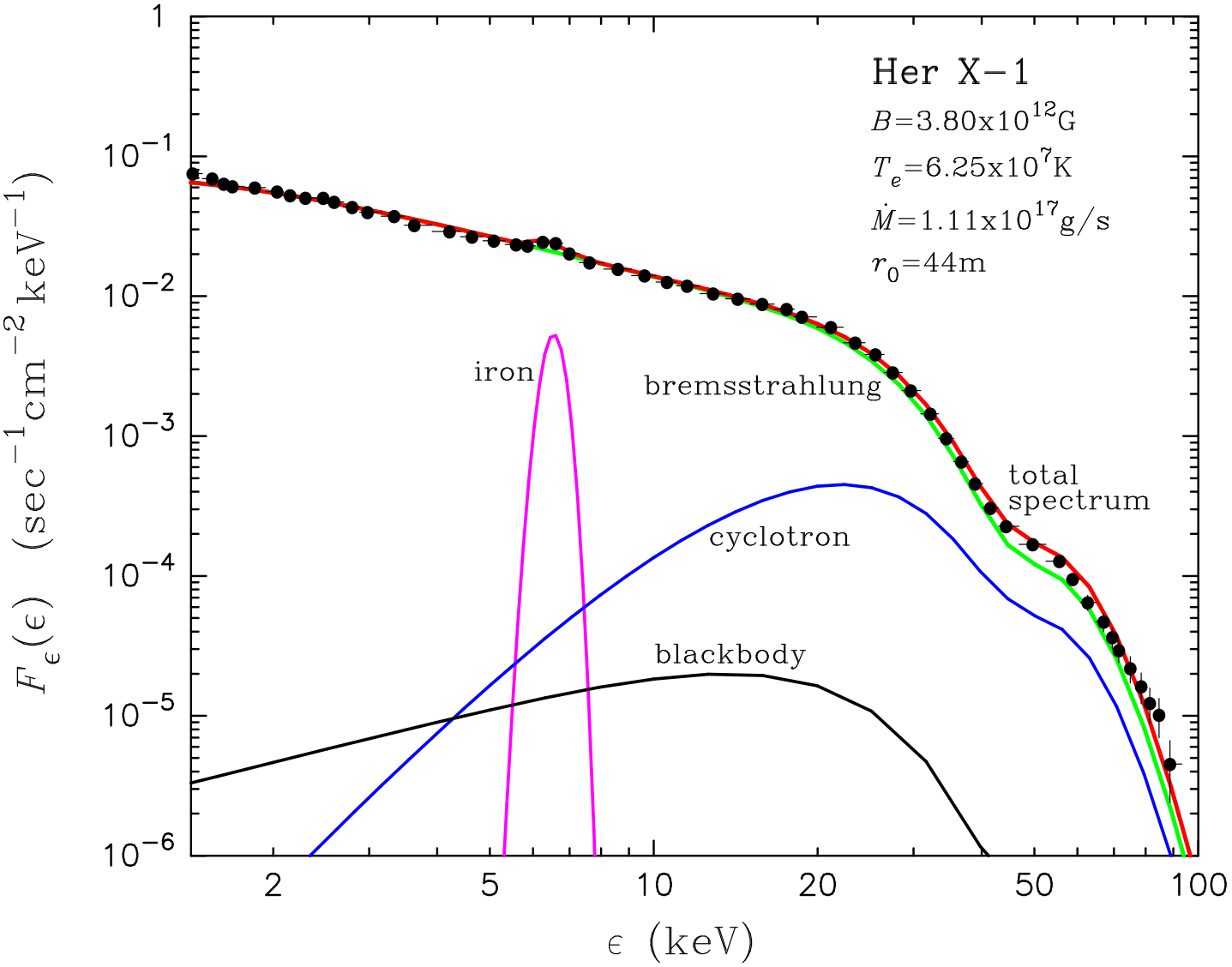

Becker & Wolff (2007, Fig. 6)

Continuum Formation: State of the Art

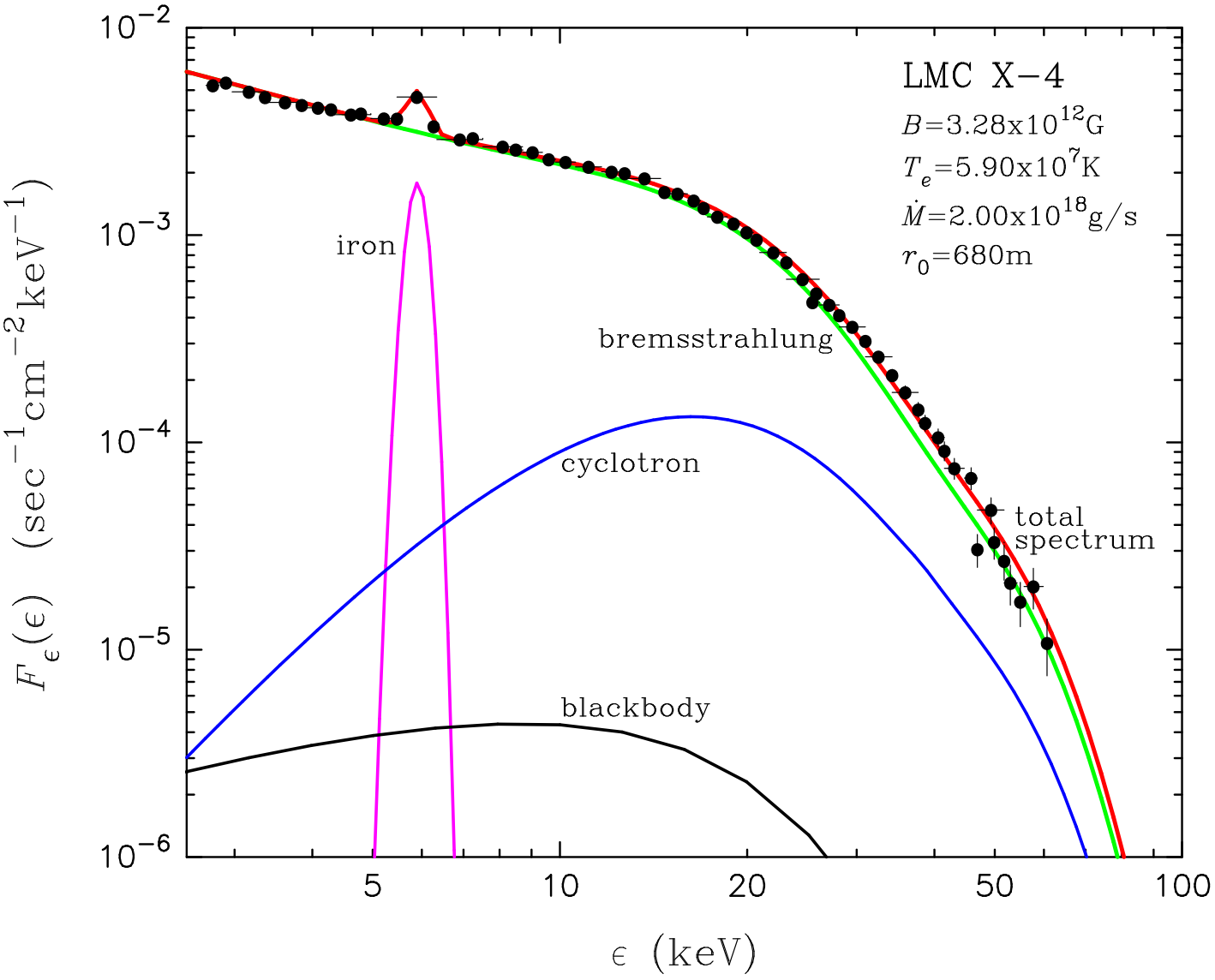

Becker & Wolff (2007, Fig. 7)

Continuum Formation: State of the Art

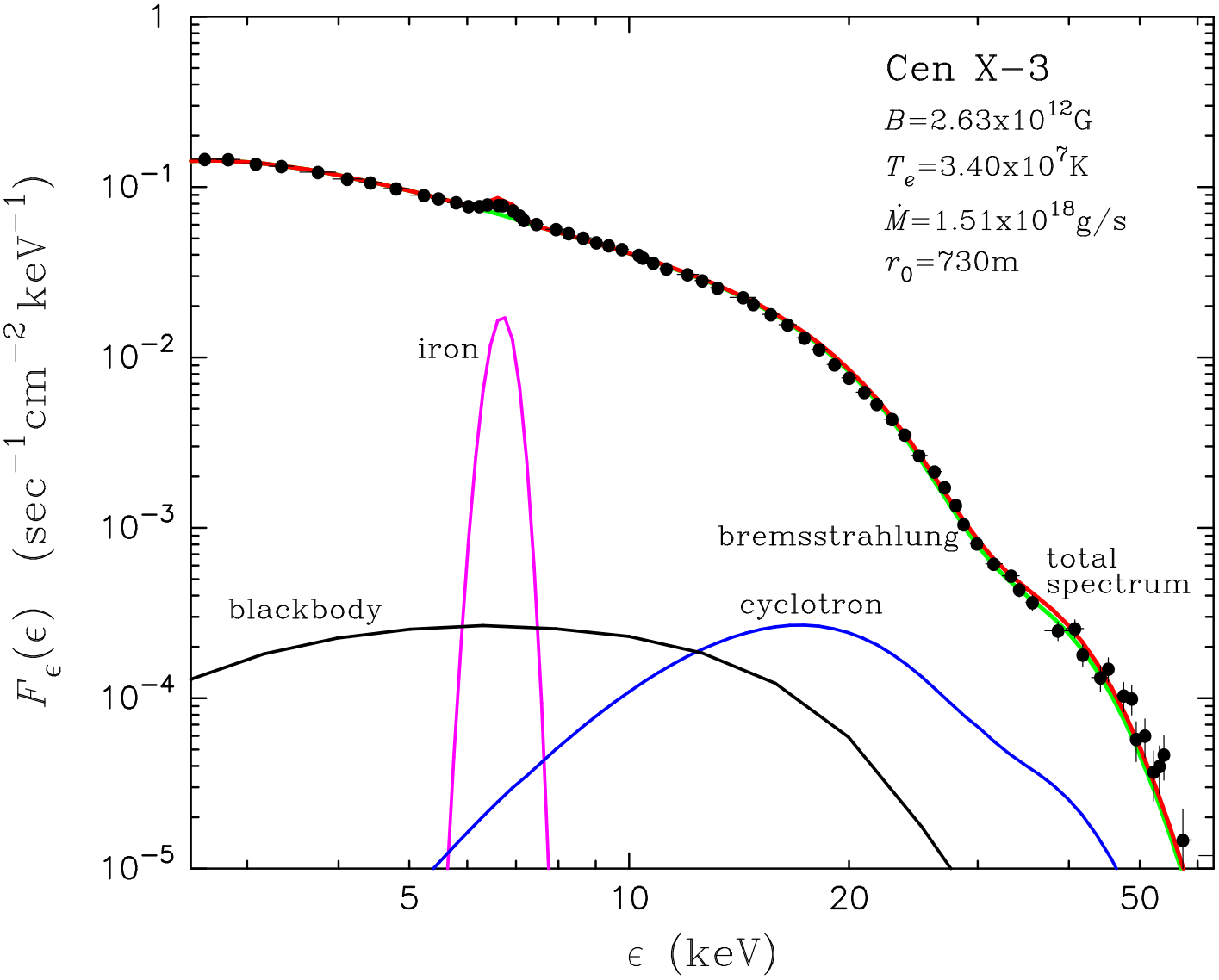

Becker & Wolff (2007, Fig. 8)

Doppler Broadening

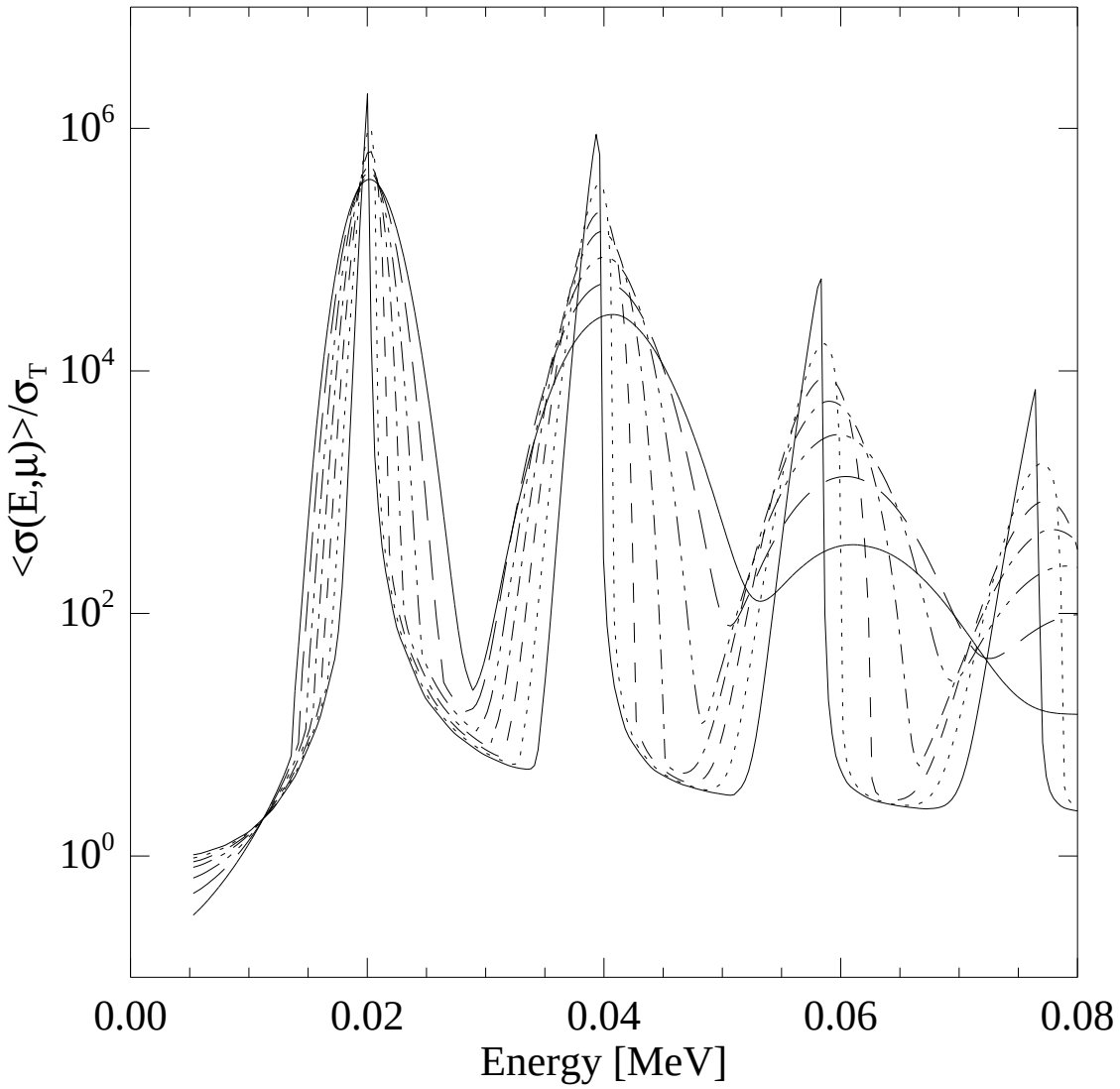

Now look at diagnostics of cyclotron lines in detail

Hot plasma

$\Longrightarrow$ thermal broadening:

- Lines narrow perpendicular to B-fi eld
- Lines broad for motion along B-fi eld

expected line width (Mészáros, 1992)

$$\frac{\Delta E_{\mathrm{FWHM}}}{E_{\mathrm{cyc}}} \sim \sqrt{kT_{\mathrm{e}}}\,|\cos\theta|$$

(~ 6 keV for $kT_{\mathrm{e}} = 40$ keV)

$B = 1.7 \times 10^{12}$ G, $kT = E_{\mathrm{cyc}}/4$, θ: angle between B-fi eld and photon direction; Schönherr et al. (2007), after Araya & Harding (1999)

Monte Carlo Simulations: Approach

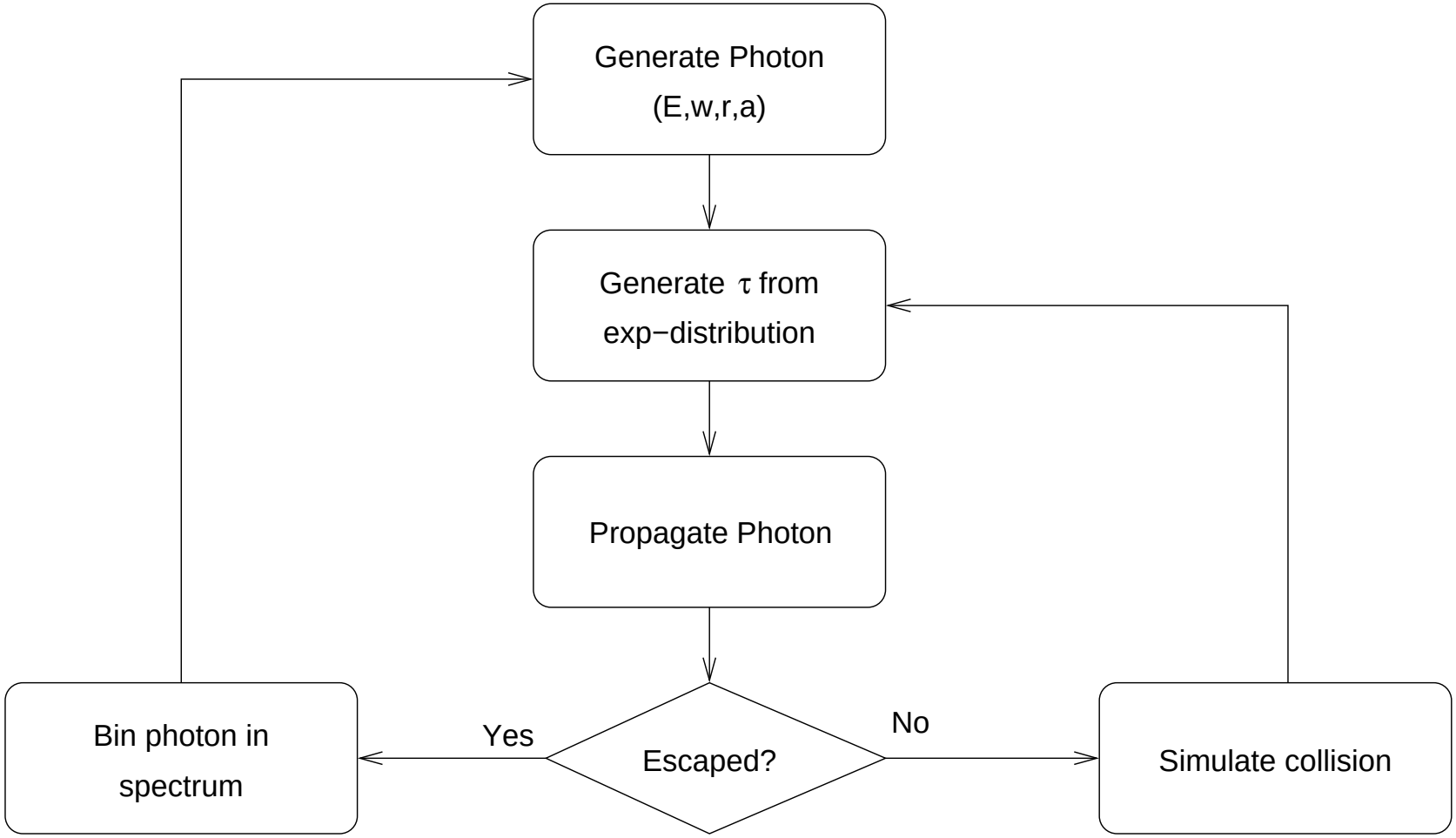

Here: use Monte Carlo approach.

Theoretical results, I

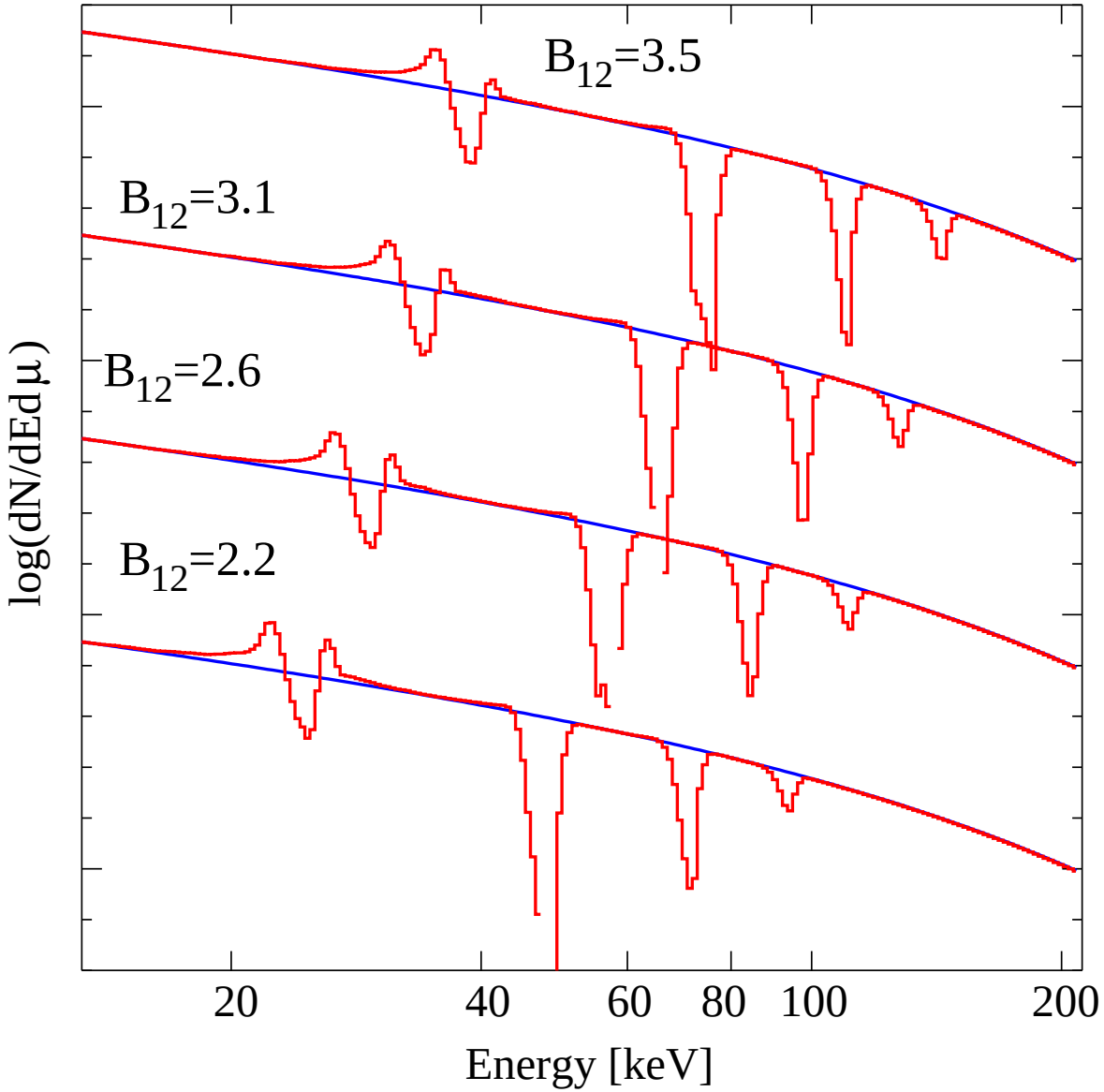

Dependence on B-field.

- Note emission wings
- Note much deeper 1st harmonic

(Schönherr et al., 2007)

Theoretical results, II

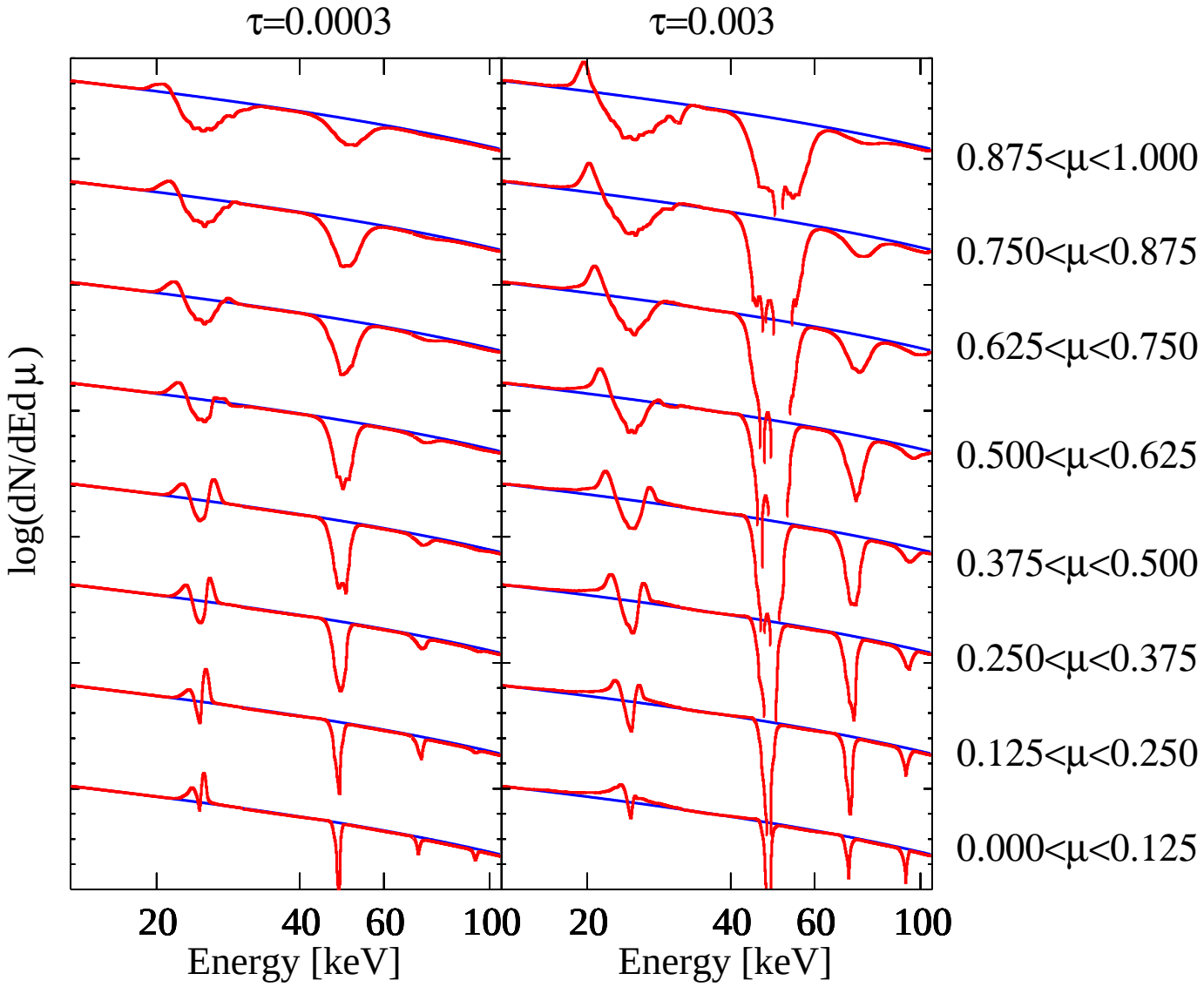

Dependence on optical depth and angle.

Note: resonance optical depth $\sim 10^5 \cdot \tau_T$!

$B = 1.76 \times 10^{12}$ G,
$kT_e = 3$ keV;
(Schönherr et al., 2007)

Theoretical results, III

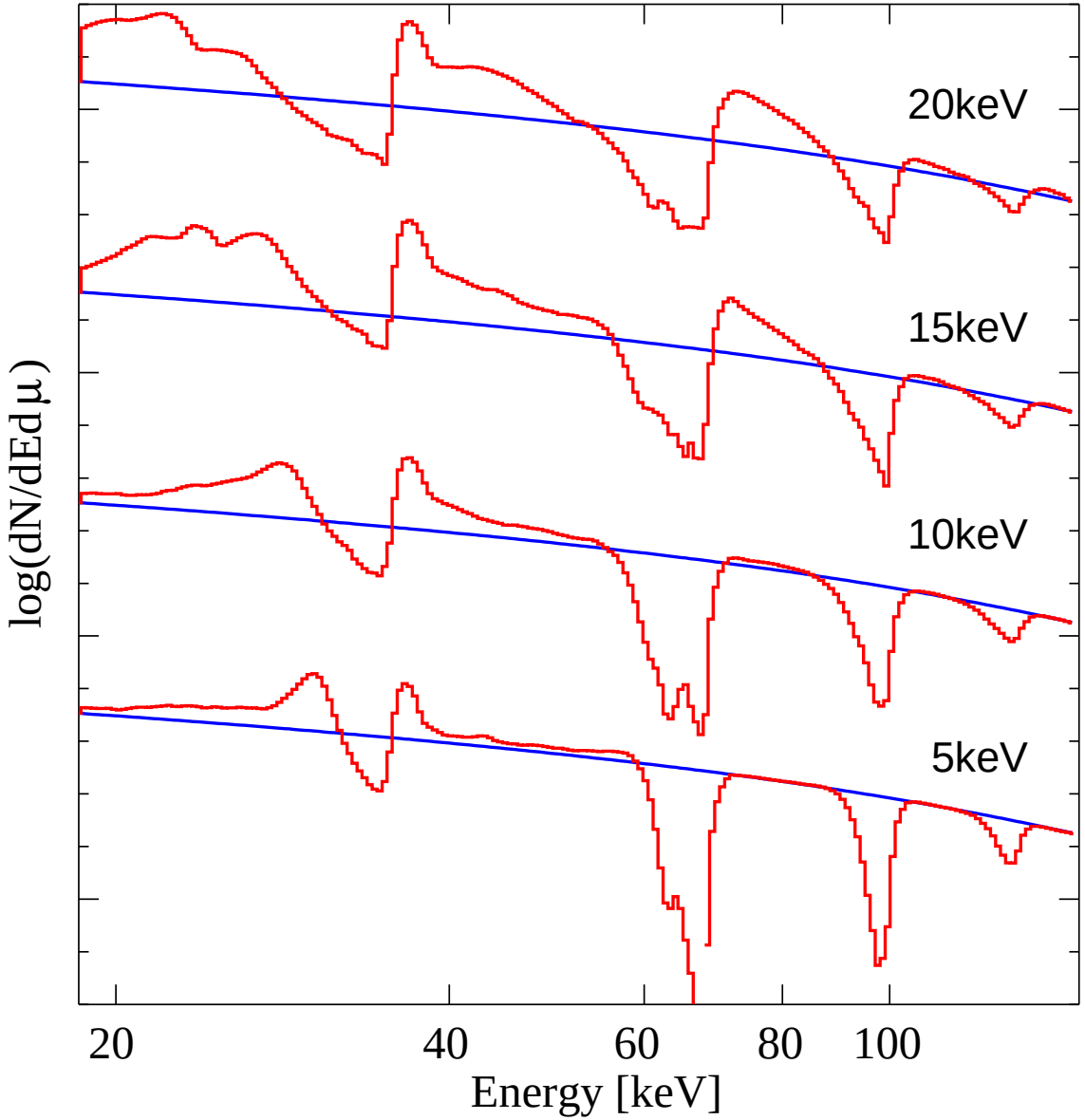

Dependence on electron temperature.

Asymmetry: relativistic Maxwellian.

(Schönherr et al., 2007)

Theoretical results, IV

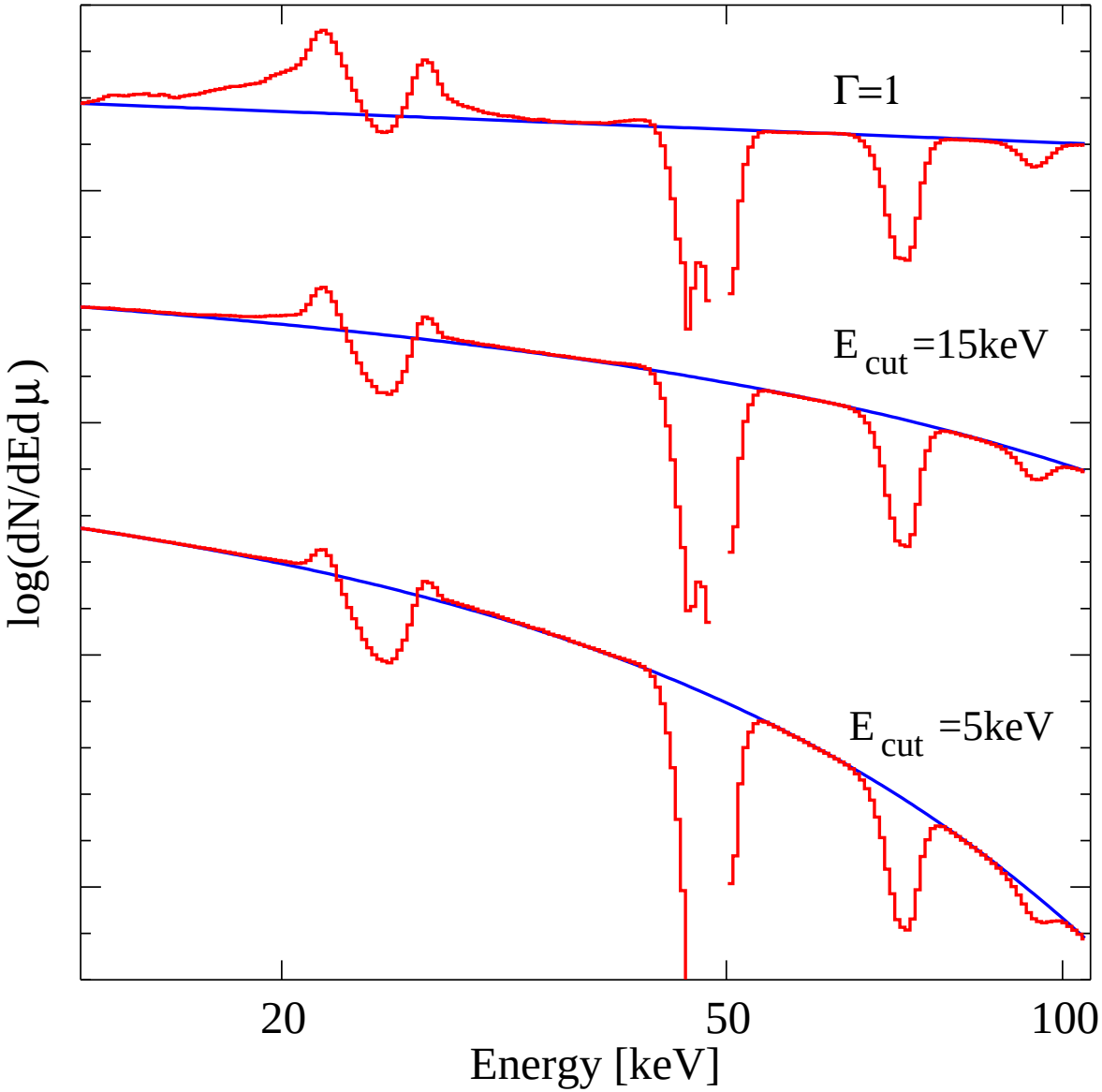

Dependence on continuum shape.

(Schönherr et al., 2007)

Cyclotron Line Sources

Source	$E_{\rm cyc}$ (keV)	$P_{\rm puls}$ (s)	$P_{\rm orb}$ (d)	companion	discovery
4U 0115+63	14, 24, 36, 48, 62	3.6	24.31	Be	HEAO-1 (Wheaton, '79) RXTE, SAX (Heindl '99, Sant.,'99)
4U 1907+09	18, 38	438	8.38	B2 III–IV	SAX (Cusumano, '98)
4U 1538−52	20	530	3.73	B0I	Ginga (Clark, '90)
Vela X-1	24, 52	283	8.96	B0.5Ib	Mir-HEXE (Kendziorra, '92), RXTE (Kreykenbohm, '02)
V 0332+53	27	4.37	34.25	Be	Ginga (Makishima, '90)
Cep X-4	28	66.25	>23	B1	Ginga (Mihara, '91)
Cen X-3	29	4.8	2.09	O6.5II	SAX (Santangelo, '98) RXTE (Heindl, '98)
X Per	29	837	250.3	B0 III–Ve	RXTE (Coburn, '01)
XTE J1946+274	36	15.8	169.2	B0-1V-IVe	RXTE (Heindl, '01)
OAO 1657−415	36?	37.7	10.4	B0-B6Ia-Iab	SAX (Orlandini, '99)
4U 1626−67	37	7.66	0.028	WD?	SAX (Orlandini, '98) RXTE (Heindl, '98)
GX 301−2	37	690	41.5	B1.2Ia	Ginga (Mihara, '95)
Her X-1	41	1.24	1.7	A9-B	Ballon-HEXE (Trümper, '78)
A0535+26	50, 110	105	110.58	Be	HEXE (Kendziorra, '92, '94), CGRO (Maisack, '97)
LMC X-4	100?	13.5	1.41	O7IV	SAX (LaBarbera, '01)

A0535+26, I

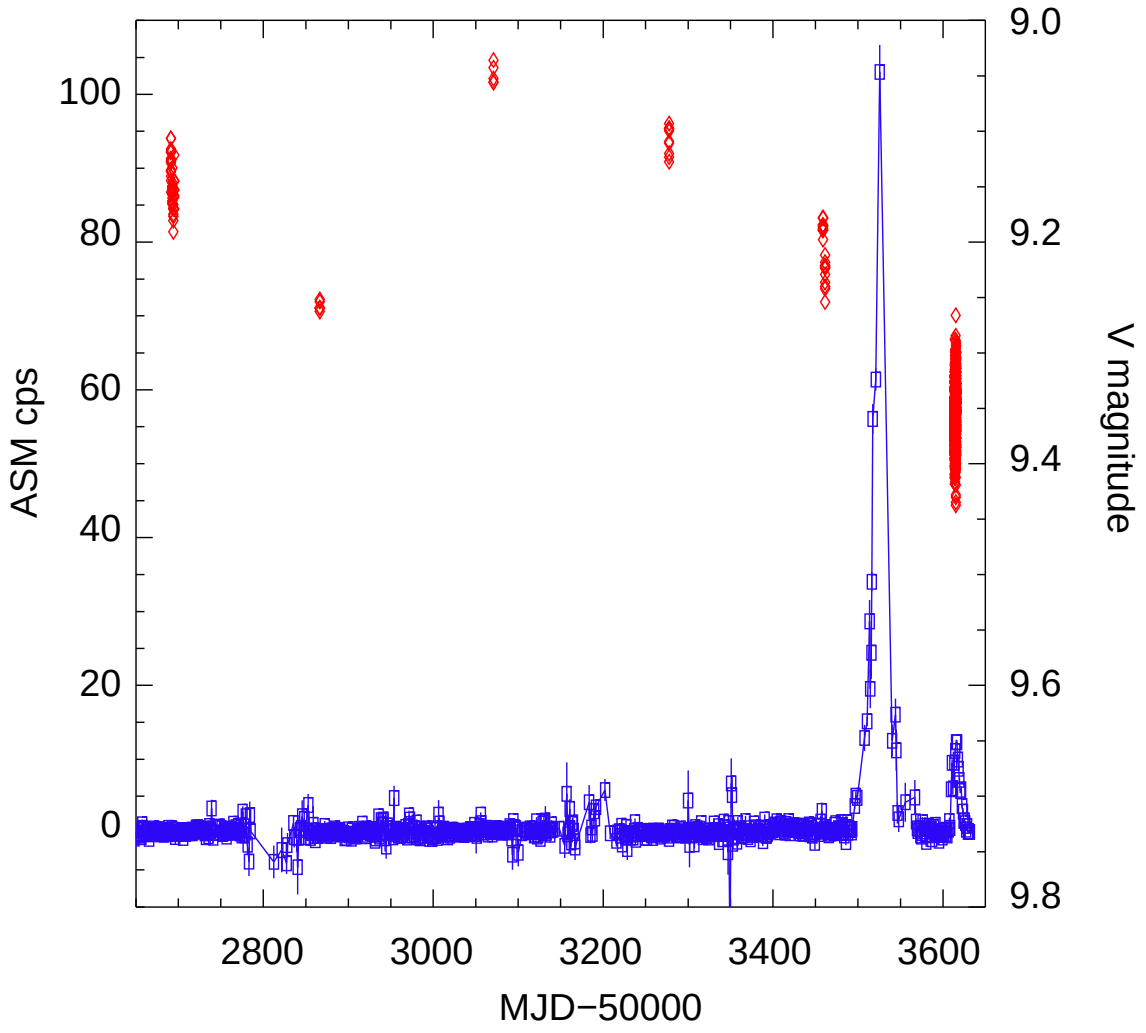

- transient O9.7IIIe/NS binary, 111 d orbit, outbursts in 1975, 1980, 1983, 1989, 1994, 2005
- giant outburst in May/June: over 1 Crab, but: too close to the Sun
- second weaker outburst: $\sim$300 mCrab in August/September, ToO observations by *INTEGRAL* and *RXTE*

A0535+26, II

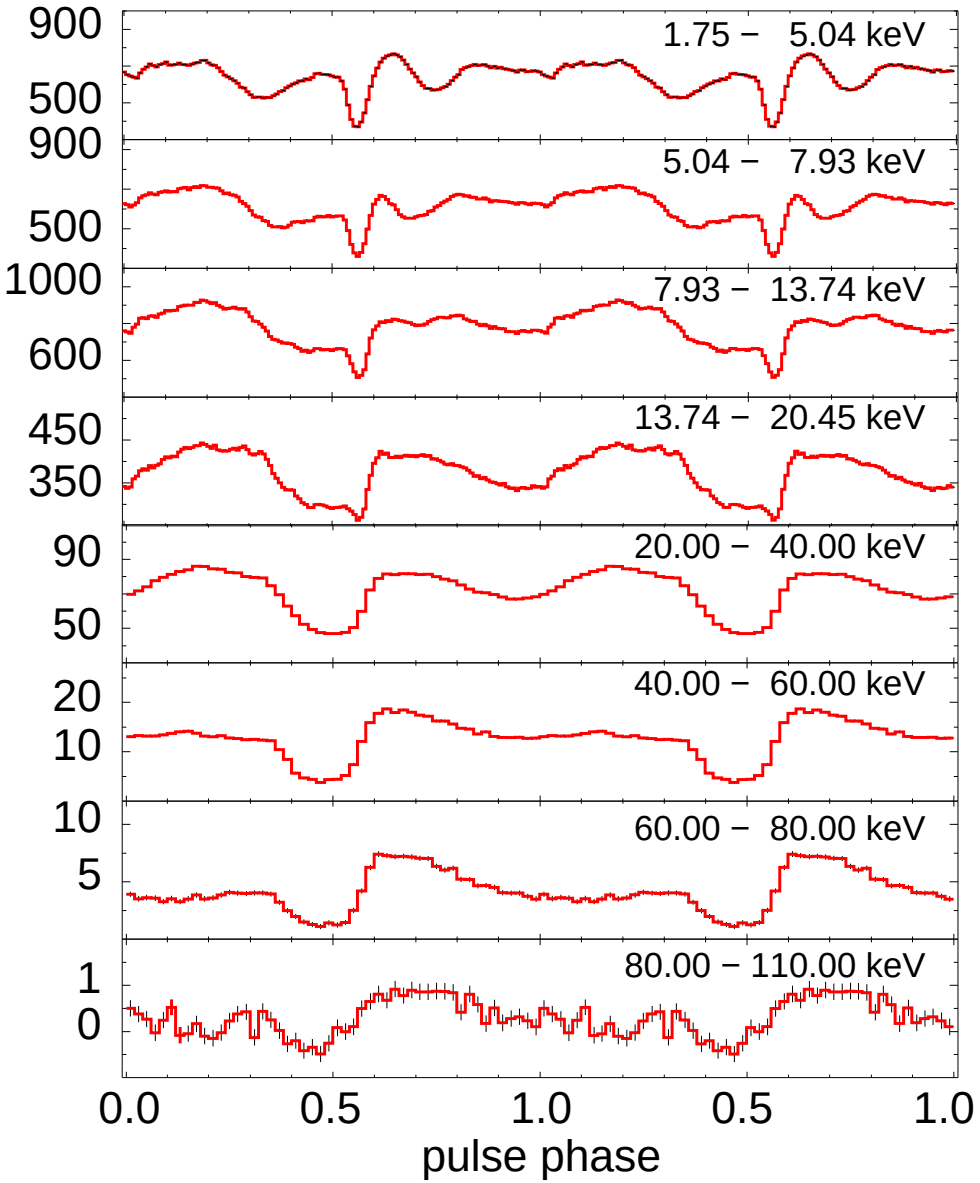

- Pulse period: $103.3920(4)$ s
- narrow feature at low energies: accretion stream?

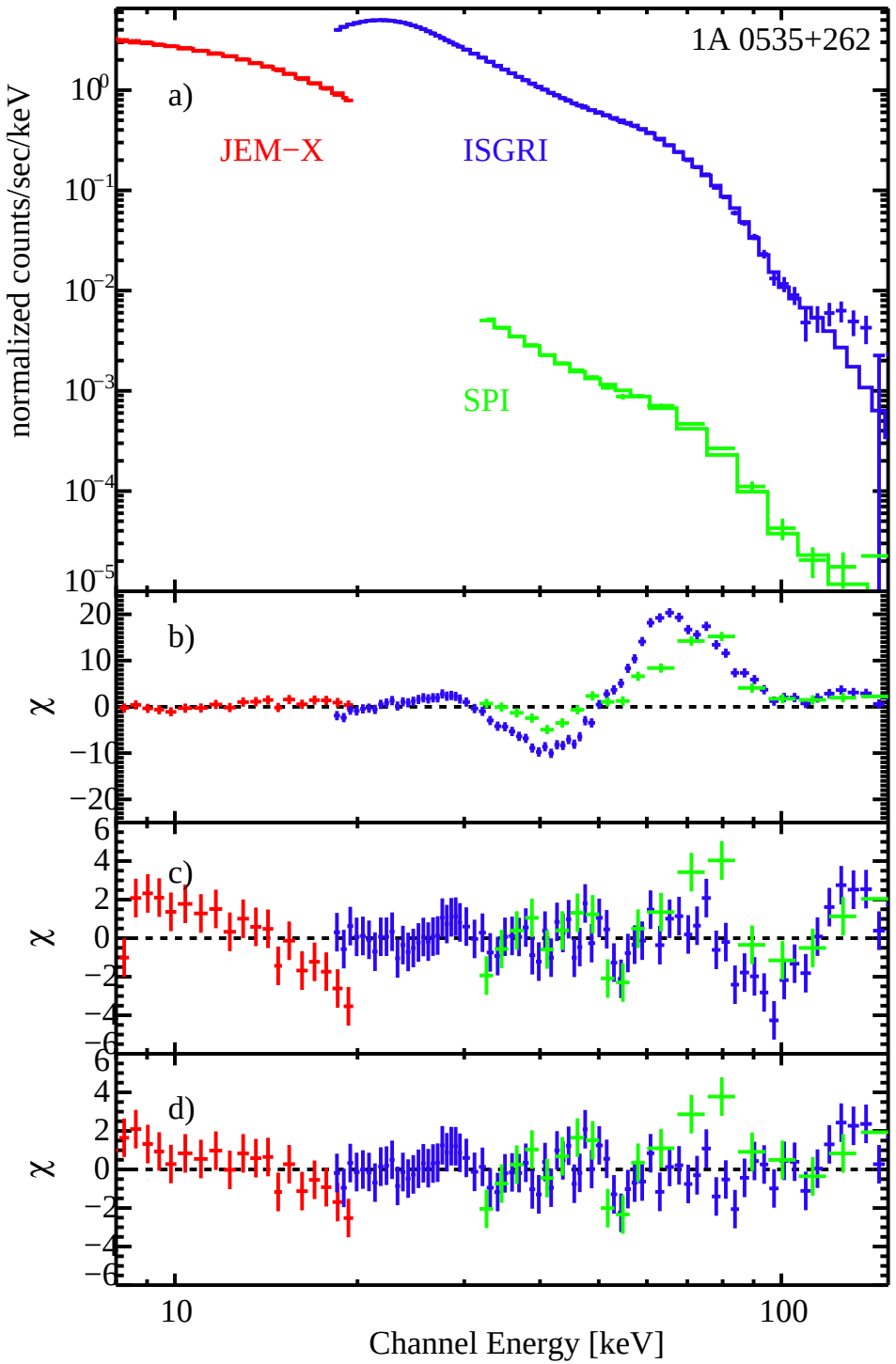

- 2 CRSFs
  - $E_{\mathrm{cyc},1} \sim 45\,\mathrm{keV}$, $\tau_1 \sim 0.5$
  - $E_{\mathrm{cyc},2} \sim 100\,\mathrm{keV}$, $\tau_2 \sim 0.6$
- *RXTE* and *INTEGRAL* consistent!

  and confi rming earlier claims for a lower line

(Caballero et al., 2007)

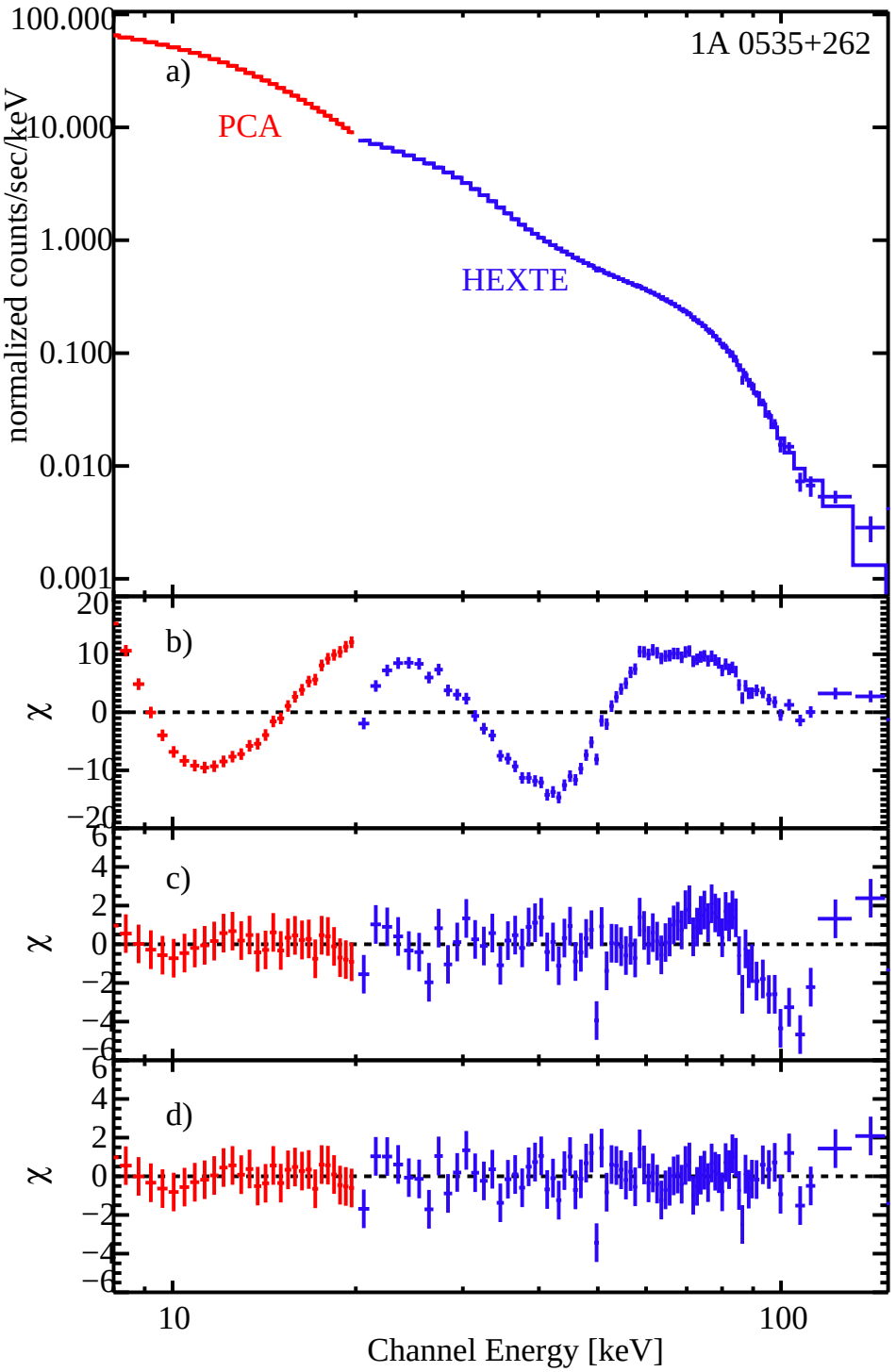

- 2 CRSFs
  - $E_{\mathrm{cyc},1} \sim 45\,\mathrm{keV}$, $\tau_1 \sim 0.5$
  - $E_{\mathrm{cyc},2} \sim 100\,\mathrm{keV}$, $\tau_2 \sim 0.6$
- *RXTE* and *INTEGRAL* consistent!

  and confi rming earlier claims for a lower line

(Caballero et al., 2007)

4U1907+09

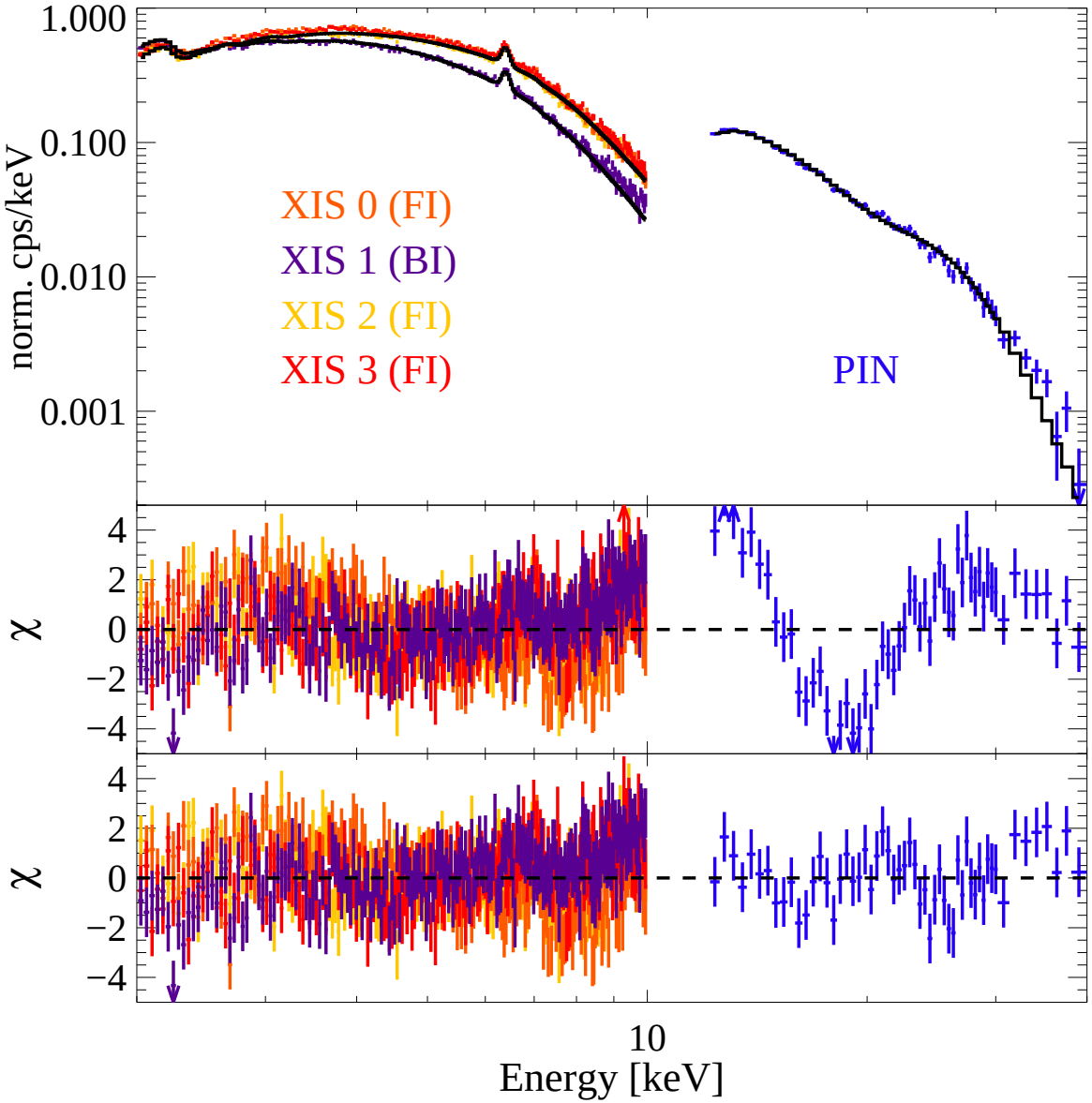

4U1907+09, 2004 December outburst: $E_{\mathrm{cyc}} = 19.7(4)$ keV, $\sigma = 3.3(3)$ keV, in agreement with earlier results (e.g., *INTEGRAL*).

Pottschmidt et al. (2007)

V0332+53

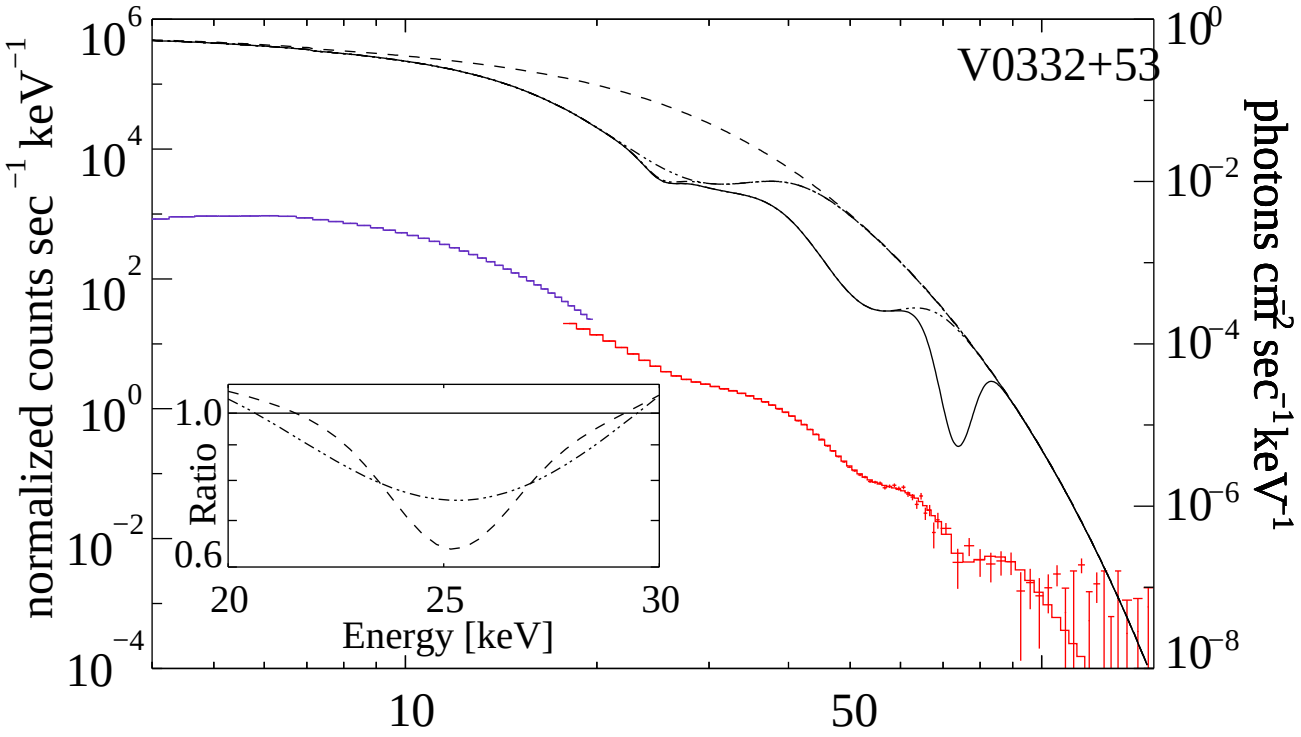

(Pottschmidt et al., 2005)

V0332+53: Cyclotron lines at 27, 51, and 74 keV; complex fundamental.

2nd source after 4U 0115+63 with more than 2 lines.

Line ratios $\neq 2$, agrees with QED prediction; also require scattering angle of $\gtrsim 60°$, in agreement with expectation from resonant cross-section.

Cen X-3

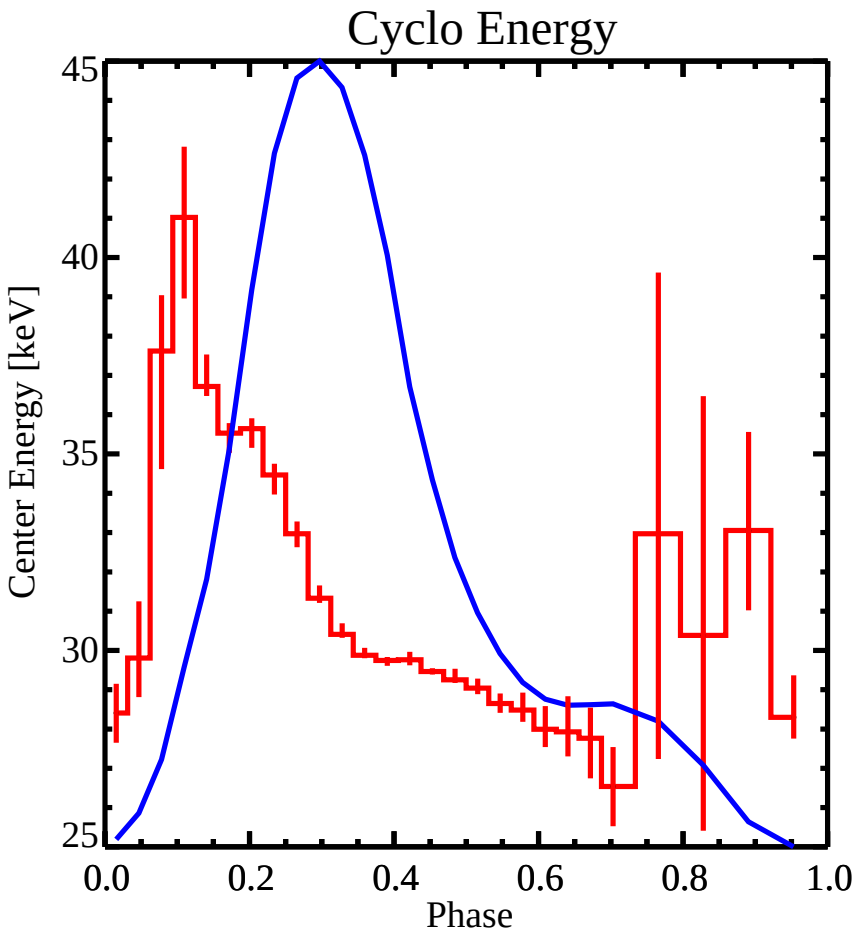

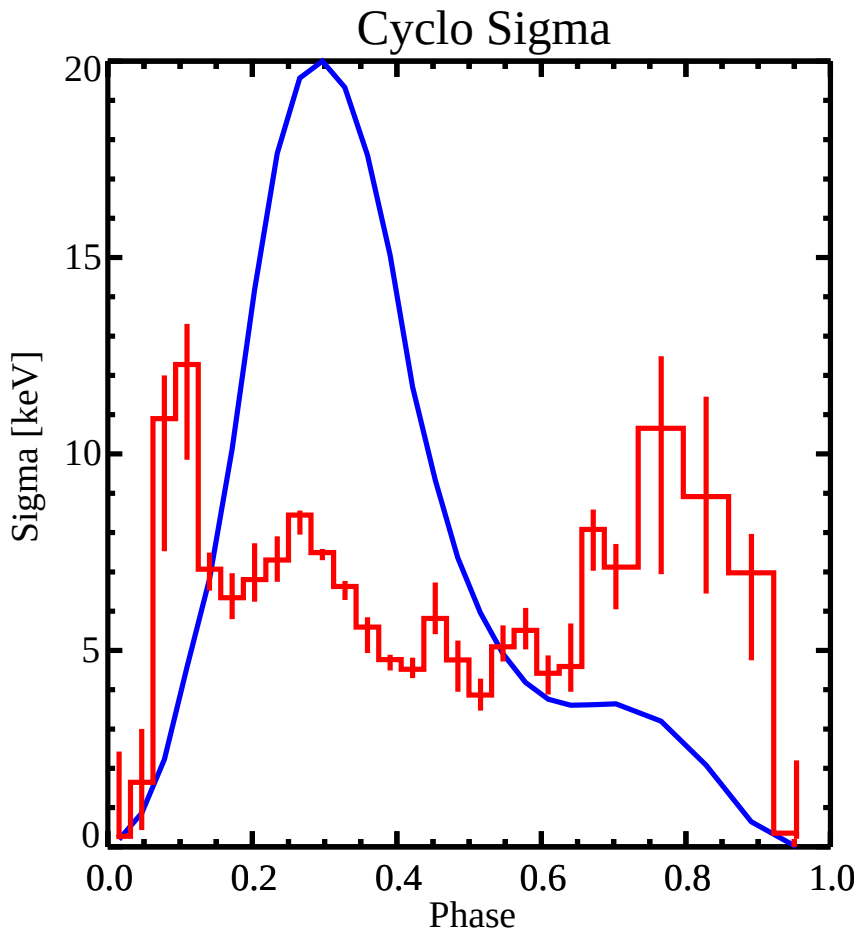

Cen X-3 (Suchy et al., in prep)

Many cyclotron sources show pulse phase dependence of line parameters.

$\Longrightarrow$ effect of viewing angle / height in accretion column?

Luminosity Dependence

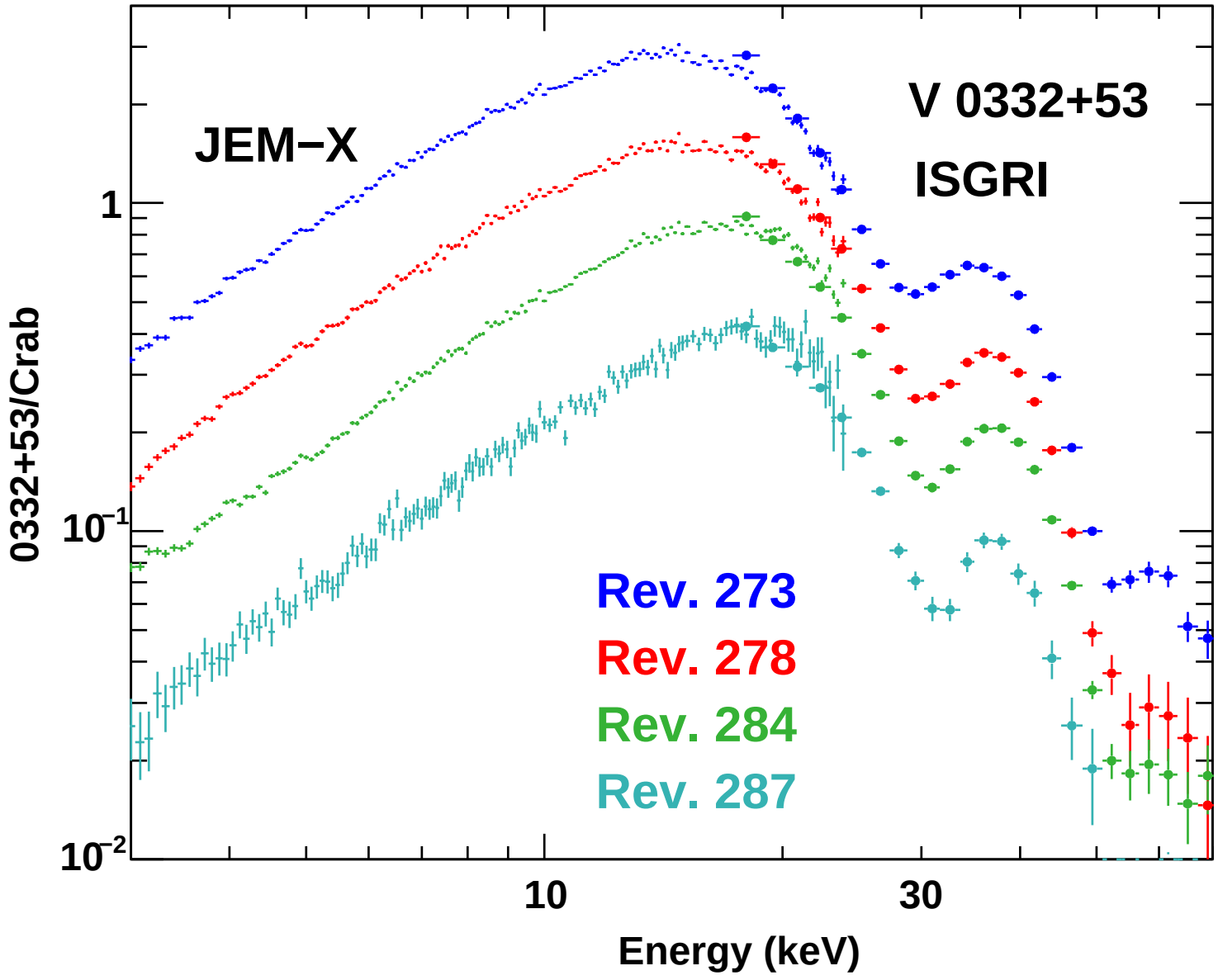

V0332+53: Energy of fundamental cyclotron line changes over outburst

(Mowlavi et al., 2006)

Luminosity Dependence

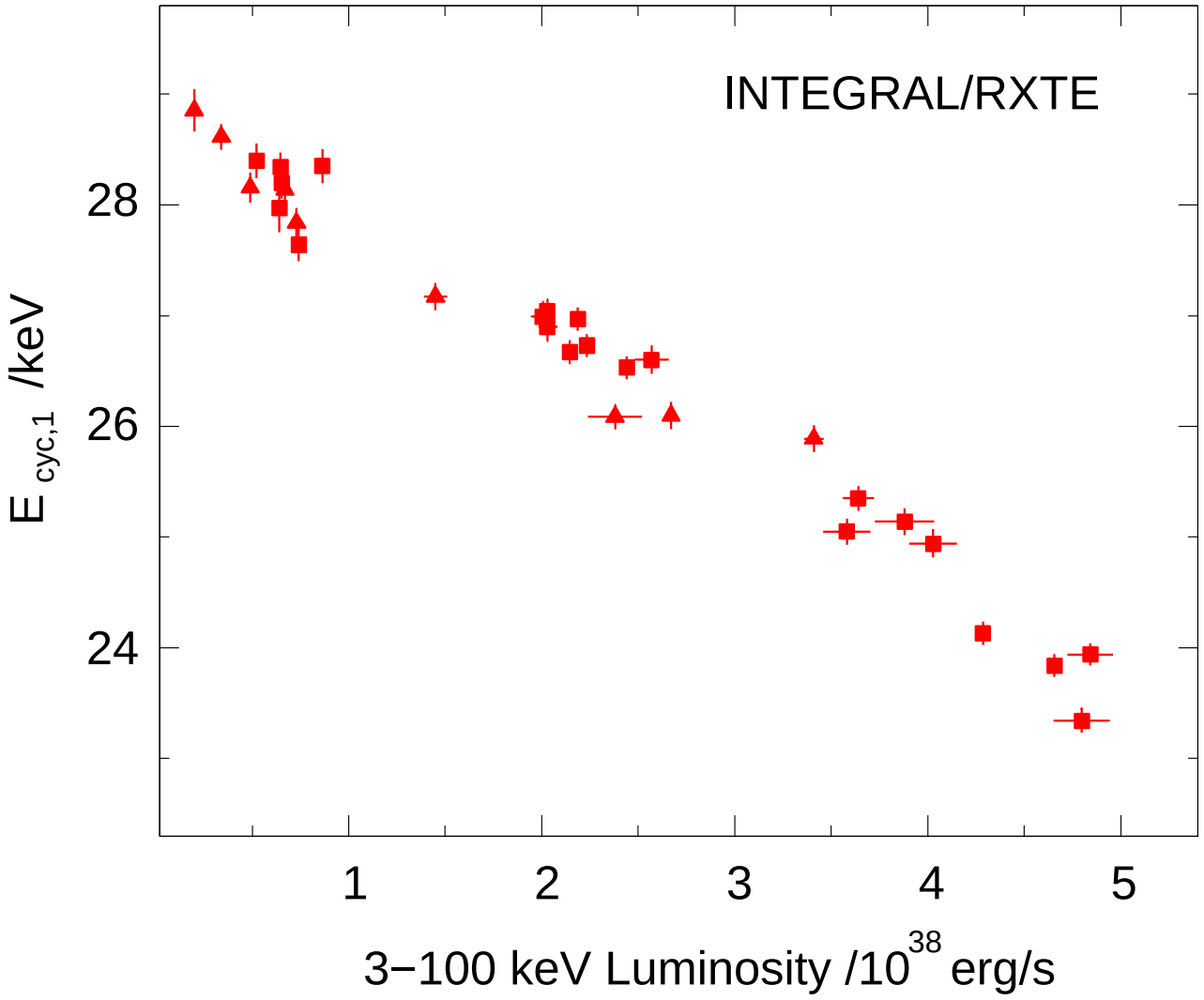

V0332+53: Cyclotron line energy depends on luminosity

$\Longrightarrow$ change of height of accretion column with $\dot{M}$

(Tsygankov et al., 2006)

Luminosity Dependence

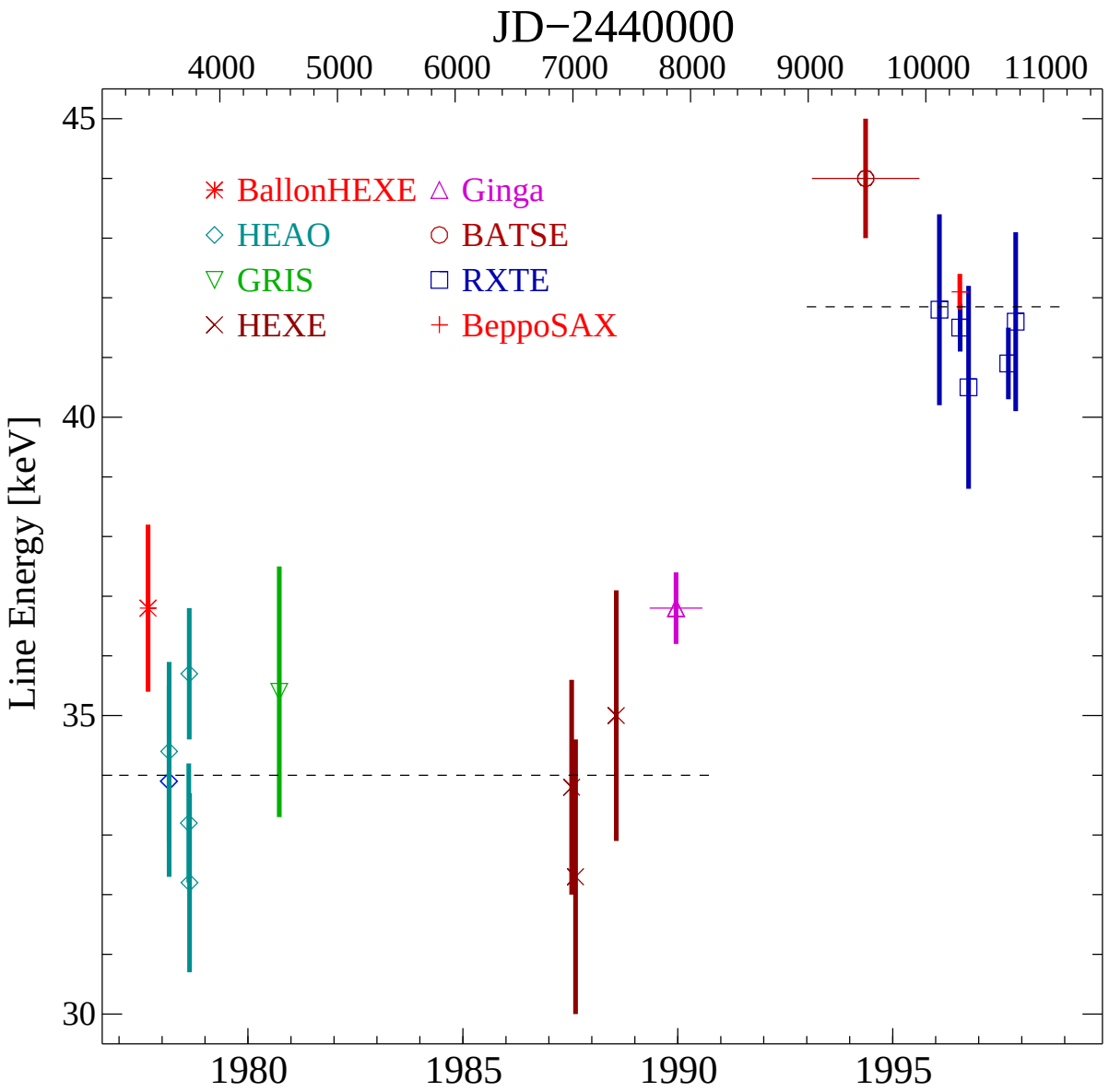

The cyclotron line in Her X-1 shows significant secular variability!

Gruber et al. (2002)

Luminosity Dependence

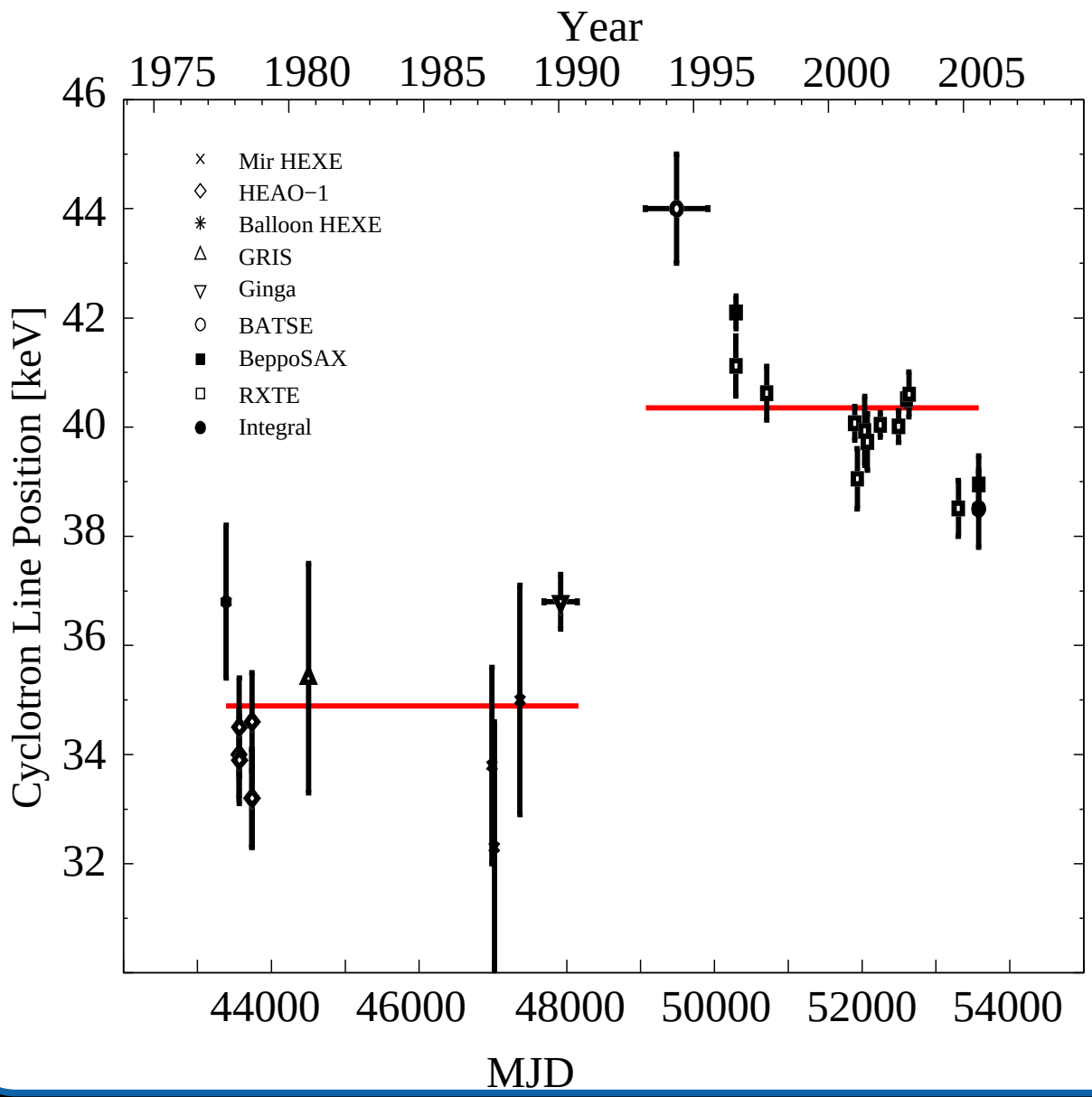

The cyclotron line in Her X-1 shows significant secular variability!

Staubert et al. (2007)

Luminosity Dependence

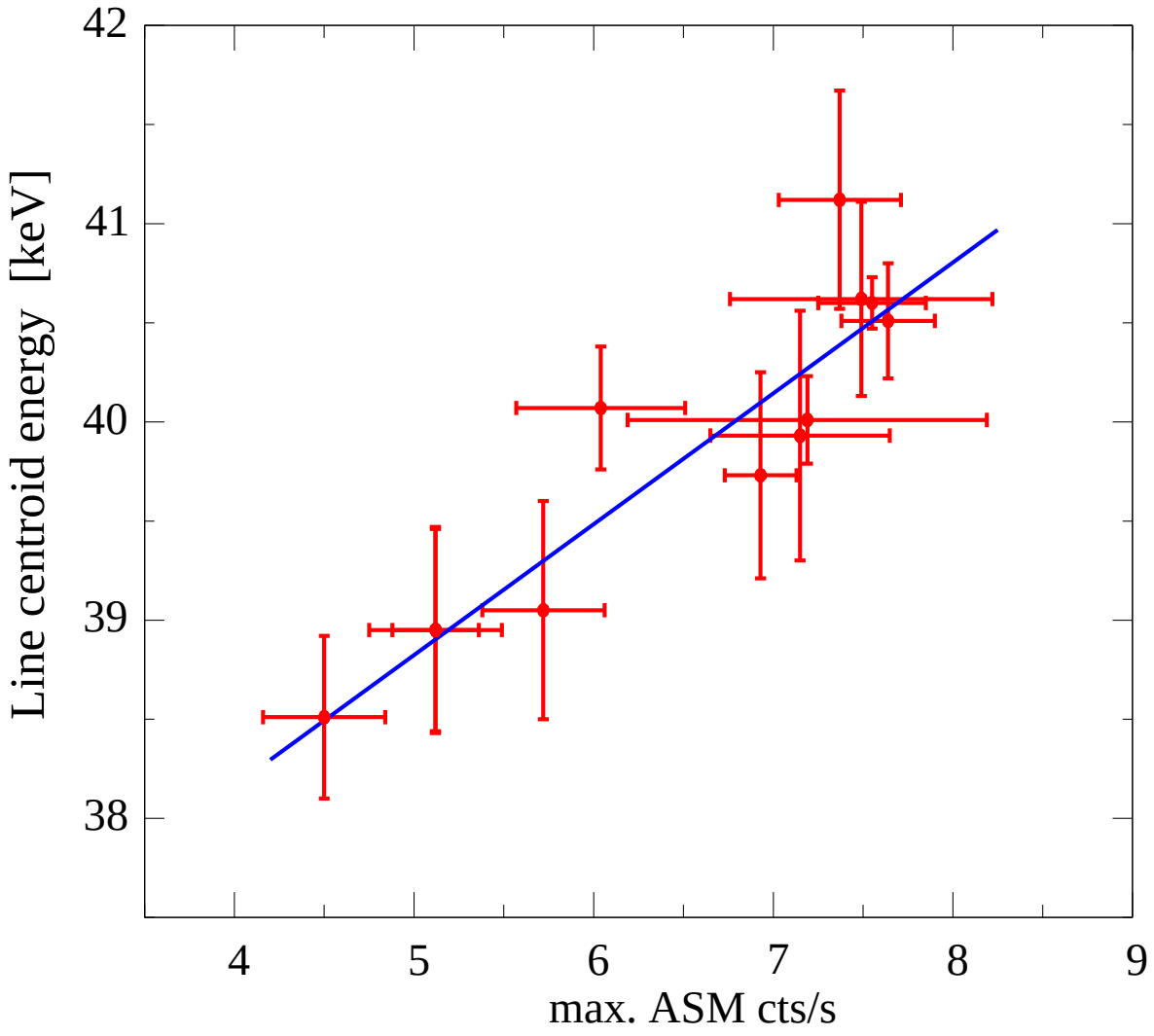

. . . but the dependence of E_{cyc} on L is different than in high luminosity sources

Her X-1: sub-Eddington source

$\Longrightarrow$ need to take structure of accretion mound into account

$\Longrightarrow$ dynamic pressure of infalling protons results in *decrease* of height of accretion mound with increasing L!

Staubert et al. (2007)

Araya, R. A., & Harding, A. K., 1999, ApJ, 517, 334

Arons, J., Klein, R. I., & Lea, S. M., 1987, ApJ, 312, 666

Basko, M. M., & Sunyaev, R. A., 1976, MNRAS, 175, 395

Becker, P. A., 1998, ApJ, 498, 790

Becker, P. A., & Wolff, M. T., 2005a, ApJ, 621, L45

Becker, P. A., & Wolff, M. T., 2005b, ApJ, 630, 465

Becker, P. A., & Wolff, M. T., 2007, ApJ, 654, 435

Bildsten, L., et al., 1997, ApJS, 113, 367

Braun, A., & Yahel, R. Z., 1984, A&A, 278, 349

Caballero, I., et al., 2007, A&A, 465, L21

Canuto, V., 1970, ApJ, 160, L153

Canuto, V., Lodenquai, J., & Ruderman, M., 1971, Phys. Rev. D, 3, 2303

Charles, P. A., & Seward, F. D., 1995, Exploring the X-Ray Universe, (Cambridge: Cambridge Univ. Press)

Davidson, K., & Ostriker, J. P., 1973, ApJ, 179, 585

Fritz, S., Kreykenbohm, I., Wilms, J., Staubert, R., Bayazit, F., Rodriguez, J., & Santangelo, A., 2006, A&A, 458, 885

Ghosh, P., & Lamb, F. K., 1979, ApJ, 232, 239

Gnedin, Y. N., & Sunyaev, R. A., 1973, A&A, 25, 233

Gonthier, P. L., Harding, A. K., Baring, M. G., Costello, R. M., & Mercer, C. L., 2000, ApJ, 540, 907

Harding, A. K., 1994, in The Evolution of X-Ray Binaries, ed. S. S. Holt, C. S. Day, (Washington: AIP), 429

Heindl, W. A., Rothschild, R. E., Coburn, W., Staubert, R., Wilms, J., Kreykenbohm, I., & Kretschmar, P., 2004, in AIP Conf. Proc. 714: X-ray Timing 2003: Rossi and Beyond, ed. P. Kaaret, F. K. Lamb, J. H. Swank, 323

Inoue, H., 1975, PASJ, 27, 311

Kreykenbohm, I., Kretschmar, P., Wilms, J., Staubert, R., Kendziorra, E., Gruber, D., & Rothschild, R., 1999, A&A, 341, 141

Langer, S. H., & Rappaport, S., 1982, ApJ, 257, 733

Mészáros, P., 1984, Space Sci. Rev., 38, 325

Mészáros, P., 1992, High-energy radiation from magnetized neutron stars, (Chicago: Chicago Univ. Press)

Mészáros, P., & Nagel, W., 1985a, ApJ, 298, 147

Mészáros, P., & Nagel, W., 1985b, ApJ, 299, 138

Mowlavi, N., et al., 2006, A&A, 451, 817

Nagel, W., 1981a, ApJ, 251, 278

Nagel, W., 1981b, ApJ, 251, 288

Ostriker, J. P., & Davidson, K., 1973, in X- and Gamma-Ray Astronomy, ed. H. Bradt, R. Giacconi, 143

Pottschmidt, K., et al., 2005, ApJ, 634, L97

Pringle, J. E., & Rees, M. J., 1972, A&A, 21, 1

Rappaport, S., & Joss, P. C., 1977, Nature, 266, 683

Schönherr, G., Wilms, J., Kretschmar, P., Kreykenbohm, I., Santangelo, A., Rothschild, R. E., Staubert, R., & Coburn, W., 2007, A&A, submitted

Trümper, J., Pietsch, W., Reppin, C., Voges, W., Staubert, R., & Kendziorra, E., 1978, ApJ, 219, L105

Tsygankov, S. S., Lutovinov, A. A., Churazov, E. M., & Sunyaev, R. A., 2006, MNRAS, 371, 19

Ventura, J., 1979, Phys. Rev. D, 19, 1684

Low-Mass X-ray Binaries